The Dissertation Committee for Caleb Frederick Sieck
certifies that this is the approved version of the following dissertation:

Bianisotropy in Passive Acoustic Metamaterials

Committee:

Andrea Alù, Supervisor

Michael R. Haberman, Co-Supervisor

Neal A. Hall

Mark F. Hamilton

Loukas F. Kallivokas

Zheng Wang

Preston S. Wilson

Bianisotropy in Passive Acoustic Metamaterials

by

Caleb Frederick Sieck, B.S.E.E.; M.S.

DISSERTATION

Presented to the Faculty of the Graduate School of

The University of Texas at Austin

in Partial Fulfillment

of the Requirements

for the Degree of

DOCTOR OF PHILOSOPHY

THE UNIVERSITY OF TEXAS AT AUSTIN

May 2017

Dedicated to Nicole

Acknowledgments

First of all, I would like to thank my advisors Professor Andrea Alù and Professor Michael R. Haberman for their always helpful advise, instruction, and support. I would also like to thank Todd Hay, Alex Athey, and John Hartman for providing financial support and teaching me valuable skills through additional projects at the Applied Research Laboratories. My understanding of acoustics has been largely shaped by the insightful instruction of Professor Mark F. Hamilton, and I would like to thank him as well as Professors Neal A. Hall, Loukas F. Kallivokas, Zheng Wang, and Preston S. Wilson for providing helpful advise and suggestions to improve this work. I was very fortunate to have many collaborations and helpful discussions with Romain Fleury and Michael B. Muhlestein. Also, I was very fortunate to be surrounded by many friends throughout this process including fellow members of Metamaterials and Plasmonics Research Group and the fellow students in the ASA-Austin student chapter. Finally, I cannot thank enough my wife and our family and friends for their continuous love and support.

Bianisotropy in Passive Acoustic Metamaterials

Publication No. _____

Caleb Frederick Sieck, Ph.D.
The University of Texas at Austin, 2017

Supervisors: Andrea Alù
Michael R. Haberman

Metamaterials are composite materials whose dynamic microstructure results in macroscopically observable properties beyond those available in nature. The emergence of metamaterials has enabled unprecedented control of electromagnetic, elastodynamic, and acoustic wave propagation and has led to technologies including invisibility cloaks, super- and hyper-lenses, and subwavelength bandgaps. These effects are made possible through the hidden degrees of freedom afforded by the dynamic microstructure. Analytically, the macroscopically observed parameters are the result of a dynamic homogenization procedure using weighted field averages over a representative volume element of the composite. After performing the homogenization procedure, constitutive relations reveal the dependencies between macroscopic fields and metamaterial properties. Recent research has demonstrated that dynamic homogenization results in constitutive relations that are coupled, which is not the case for most traditional materials. This general effect is well-known in

electromagnetism and is known as bianisotropy, but the analogous effect in elastodynamics and acoustics was discovered more recently and is also often referred to as Willis coupling. However, most current homogenization schemes are modeled to determine macroscopic properties in the same form as traditional materials and therefore do not account for coupled constitutive relations. Additionally in the absence of embedded sources, metamaterial parameters are non-unique, which allows for macroscopic descriptions that only include traditional parameters or traditional parameters and coupling parameters. For acoustic metamaterials, the traditional properties are density and compressibility. The additional coupling parameters result in macroscopic momentum density and volume strain fields that are coupled due to both being dependent on macroscopic acoustic particle velocity and pressure fields. This dissertation explores the analogs between bianisotropy in electromagnetism, elastodynamics, and acoustics and the consequences of neglecting these effects on the physical interpretation of acoustic metamaterial parameters. The analogs are used to provide a qualitative understanding of the origin of coupling parameters, and a multiple scattering homogenization procedure is derived to demonstrate coupling due to asymmetry and nonlocal effects. Additionally, the restrictions of causality, passivity, and reciprocity on acoustic metamaterial parameters are derived, and it is demonstrated that macroscopic descriptions that neglect bianisotropy in one-dimensional acoustic metamaterials do not in general satisfy these restrictions.

Table of Contents

List of Figures

Chapter 1

Introduction

1.1 Metamaterials

Metamaterials are composite materials with macroscopically observable properties beyond those available in nature. The ability to engineer these composites to have extreme material properties has enabled the control of electromagnetic, elastodynamic, and acoustic waves in unprecedented ways. The field of metamaterials began with three seminal works published in 2000: Pendry's explanation of a perfect lens [1], Smith *et al.*'s demonstration of a double negative medium [2], and Liu *et al.*'s demonstration of negative mass density [3] (although they initially thought it was negative stiffness). While these works began the flood of research, recent metamaterial reviews have demonstrated that such composites are more than a century in the making, finally made possible by advances in manufacturing and computation [4–6]. The goal of these composites has always been to achieve ideal constitutive properties for applications such as scattering reduction, isolation, and enhanced imaging. Towards these ends, metamaterials have enabled cloaking [7], low frequency bandgaps [3], and super- and hyper-lenses [8].

For acoustics, the material properties of interest are the dynamic bulk

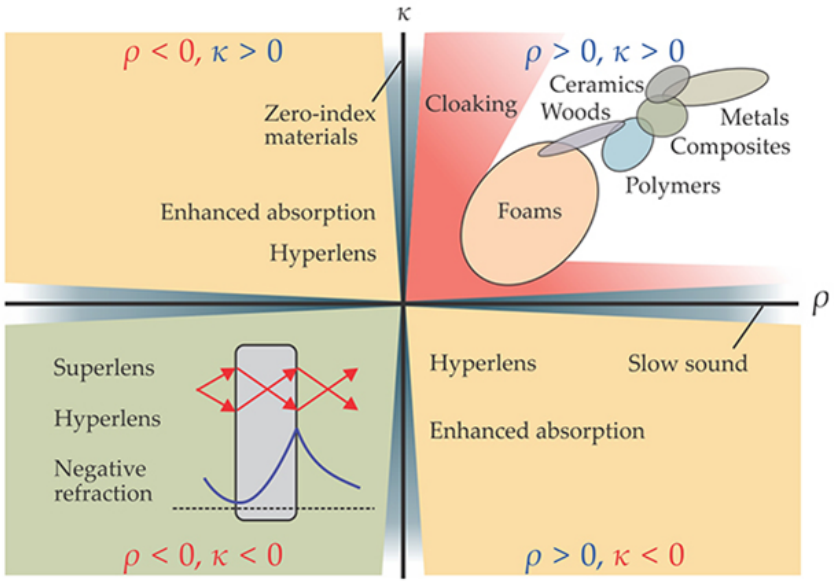

Figure 1.1: Ashby chart depicting the expanded range of mass density ρ and bulk modulus κ made possible with acoustic metamaterials. Adapted from [9], with the permission of the American Institute of Physics.

modulus κ (or compressibility $\beta = 1/\kappa$) and mass density ρ, which give rise to wave properties, phase speed $c = \sqrt{\kappa/\rho}$ and characteristic impedance $Z = \sqrt{\rho\kappa}$ [6, 10, 11]. The space of possible properties is often illustrated on an Ashby chart such as Figure 1.1, which displays the acoustic properties with κ on the vertical axis and ρ on the horizontal axis [9]. The properties of natural materials and static properties of composites occupy the first quadrant where $\kappa > 0$ and $\rho > 0$. All other regions of the chart are only accessible with metamaterials, in which case κ and ρ represent dynamic—frequency dependent—quantities not static quantities. Using metamaterials, it is possible to achieve exotic media exhibiting zero index with $\rho \to 0$, low sound speed with $\kappa \to 0$, evanescence for $\rho < 0$ or $\kappa < 0$, negative phase speeds for

$\rho < 0$ and $\kappa < 0$, and recently, double zero refractive index with $\rho \to 0$ while $\kappa \to \infty$ [12]. The dynamic properties of metamaterials are in fact effective material properties which describe macroscopic wave phenomena at a particular frequency. They are effective because they are the result of the responses and interactions of subwavelength microstructures. It is the goal of acoustic metamaterials research to explore the feasibility of developing and applying these exotic, dynamic properties [10, 11].

1.2 Motivations

Metamaterials are composite materials that rely on engineered microstructures to achieve extreme macroscopic properties. Therefore, the realization of metamaterials for electromagnetic, elastodynamic, and acoustic waves required the exploration of dynamic homogenization schemes to accurately predict the metamaterial properties [13–21]. A valid homogenization scheme must accurately relate the dynamic response of microscopic inhomogeneities and their interactions at the mesoscale to realize metamaterials with exotic macroscopic parameters exhibiting very large, vanishingly small, and negative values. Additionally, the homogenization scheme should satisfy applicable physical constraints, such as those due to passivity and reciprocity, and be independent of the specific setup in which the metamaterial is tested [22–24]. One critical result of dynamic homogenization, often neglected due to quasi-static assumptions, is the existence of coupling terms in constitutive relations [16]. The concept of coupled constitutive relations is well known in

electromagnetism, and it is generally referred to as bianisotropy or magnetoelectric coupling [25, 26]. In contrast, analogous field coupling or bianisotropy in elastodynamics and acoustics has only recently begun to receive attention, and it is also commonly referred to as Willis coupling in honor of J. R. Willis who demonstrated in the 1980s that field coupling is a general result of dynamic homogenization [27–31].

In traditional media, constitutive relations associate fields whose inner product yields either the potential or kinetic energy at a material point. Potential energy is calculated from the inner product of the electric field and electric displacement in electromagnetism, stress and strain in elastodynamics, and pressure and volume strain in acoustics, and kinetic energy is calculated from the inner product of the magnetic field and magnetic flux in electromagnetism and particle velocity and momentum density in both elastodynamics and acoustics. Additionally, energy is converted from one form to the other in wave propagation, which is described through dynamic equations that couple fields from the two sets just defined. For example, the linear conservation of momentum, $\nabla\hat{p} = -\dot{\hat{\boldsymbol{\mu}}}$, (discussed in Section 3.2) is a dynamic equation that relates acoustic pressure $\hat{p}$, associated with potential energy, to acoustic momentum density $\hat{\boldsymbol{\mu}}$, associated with kinetic energy. In bianisotropic media, constitutive relations are coupled and therefore contain fields associated with both potential and kinetic energy. This coupling between constitutive relations implies energy conversion in the material response to a particular field, which is distinct from the exchange of energy that occurs in wave propagation.

Macroscopic coupled constitutive relations may result from several dynamic microscale and mesoscale effects including chiral inhomogeneities [26, 32, 33], asymmetric inhomogeneities and substrate effects [15, 17, 24, 34–39], nonlocal effects due to finite phase speed and multiple scattering [15, 19, 20, 40, 41], and nonreciprocal biases [25, 26, 42–44]. Related coupling mechanisms also occur in elastic media including "Cosserat media" in which a static strain produces a rotation and in acoustic propagation through porous/poroelastic media.

Despite the prevalence of published work in bianisotropy and Willis coupling, the physical analogies between the origins of these effects in electromagnetic and elastic systems has not been fully discussed. Additionally, while a few works have provided exact theoretical validations of Willis coupling [17, 19, 37, 38], the methods used do not provide a clear picture of the underlying physics. Finally, in the absence of sources, constitutive relations are non-unique [14–16]. However, not all macroscopic descriptions yield physically meaningful properties [22–24, 40]. This work addresses these considerations by (*i*) highlighting useful analogies between electrodynamic, elastodynamic, and acoustic systems, (*ii*) deriving physical restrictions on macroscopic parameters, (*iii*) deriving a new source-driven, multiple scattering homogenization procedure that demonstrates the physical origins of Willis coupling in acoustic metamaterials, and (*iv*) providing numerical examples demonstrating that bianisotropy must be taken into account in order for macroscopic parameters to satisfy physical restrictions.

1.3 Overview

This dissertation is organized as follows. Chapter 2 provides a brief perspective on the connection between bianisotropy in electromagnetism and Willis coupling in elastodynamics, highlighting important physical analogies and qualitative examples. The remainder of the work focuses on bianisotropy in acoustic metamaterials, which was inspired and guided by analogous work in electromagnetism, most notably the works of Alù [15, 23] and Simovski [22, 45]. Chapter 3 presents physical restrictions on macroscopic acoustic parameters based on passivity, reciprocity, and causality. These restrictions will be used in Chapters 4 and 5 to assess the validity of the multiple-scattering homogenization theory advanced by the present work.

In Chapter 4, a self-consistent, multiple scattering homogenization procedure provides an intuitive demonstration of the origins of macroscopic coupling in acoustic metamaterials. The homogenization procedure results in exact solutions for 1D periodic media, which are discussed in detail in Chapter 5. Additionally, due to their non-uniqueness, the derived *effective* parameters are compared to two additional macroscopic models: *equivalent* parameters which neglect coupling, and *Bloch* parameters which relate microscopic or exact fields at unit cell boundaries rather than effective fields. Three example 1D periodic media are considered, and the *effective*, *equivalent*, and *Bloch* parameters are discussed in light of physical restrictions. The findings were recently verified through experimental efforts by the author and colleagues. The experiment is reported in detail by Muhlestein [46] and Muhlestein *et al.* [47]. Finally,

conclusions and suggestions of future research are provided in Chapter 6.

Chapter 2

Bianisotropic Media

This chapter provides an introduction to bianisotropy in electromagnetism, elastodynamics, and acoustics and highlights useful analogies between these wave phenomena. Qualitative examples are discussed to demonstrate the microscopic and mesoscopic origins of bianisotropy using fundamental physics. Bianisotropic media is distinguished from traditional media by the presence of field coupling in the constitutive relations. Section 2.1 provides a brief introduction and history of the known microscopic physical mechanisms leading to macroscopically observable bianisotropy in electromagnetism, as well as an example of how bianisotropy may be introduced at the microscale by an asymmetric inhomogeneity. Section 2.2 provides an overview of work in elastodynamics and acoustics involving coupled constitutive relations, an example of a coupled response from an asymmetric inhomogeneity in an acoustic pressure field, and a qualitative discussion of nonlocal coupling. In order to clarify the discussion, variables common to each discipline—electromagnetism, elastodynamics, and acoustics—are used. As such, variables only in Section 2.1 refer to the electromagnetic definitions; variables only in Section 2.2 refer to elastodynamics; and variables in the remainder of this work refer to acoustic definitions that are provided wherever defined. Also, the $e^{-i\omega t}$ time convention

is assumed for all complex expressions.

2.1 Bianisotropy in electromagnetism

The study of bianisotropic media in electromagnetism has a long history, with inquiry stretching back over 200 years [26, 32]. The term "bianisotropic" was proposed in 1968 by Cheng and Kong [48] to describe a material that displays an electrical response resulting from both electric and magnetic excitation and a magnetic response resulting from both magnetic and electric excitation, and in general, the response is not parallel to either excitation. This behavior is represented by the constitutive relations provided in Equation (2.1). A variety of physical effects may be efficiently modeled in the frequency domain using bianisotropic constitutive relations, and knowledge of their origins provides key insight into understanding bianisotropy in the dynamic response of elastic and acoustic media. The general bianisotropic constitutive relations in electromagnetism can be expressed in indical notation as

$$\begin{aligned} D_i &= \varepsilon_{ij} E_j + \zeta_{ij} H_j, \\ B_i &= \xi_{ij} E_j + \mu_{ij} H_j, \end{aligned} \tag{2.1}$$

where the electric and magnetic field strengths, $\boldsymbol{E}$ and $\boldsymbol{H}$, and the electric and magnetic displacements, $\boldsymbol{D}$ and $\boldsymbol{B}$, are all vectors, and the four material parameters, electric permittivity $\underline{\boldsymbol{\epsilon}}$, magnetic permeability $\underline{\boldsymbol{\mu}}$, and two coupling parameters $\underline{\boldsymbol{\zeta}}$, and $\underline{\boldsymbol{\xi}}$ are all second order tensors. Restrictions on the parameter tensors based on symmetry, time and spatial inversion, reciprocity, and passivity were first formally expressed by Kong [25].

The earliest observed effect which can be modeled with bianisotropic relations dates back more than 200 years and is known as optical activity. This phenomenon occurs naturally in some crystals and is marked by the rotation of linearly polarized light as it propagates through a material [26, 32]. Media with optical activity are reciprocal, and materials demonstrating this response are generally referred to as chiral media. In 1914, Lindman demonstrated that chirality could be achieved at microwave frequencies by using a composite containing subwavelength copper helices [49]. In the mid-20th century, Landau and Lifshitz predicted a coupling phenomenon in antiferromagnetic materials that they called the magnetoelectric effect [50]. Unlike chirality, the magnetoelectric effect is nonreciprocal [26]. An engineered version of nonreciprocal coupling was demonstrated by Tellegen in 1948 using the circuit element he called a gyrator [42]. Propagation in general bianisotropic media, containing reciprocal and nonreciprocal features, continued to be studied extensively throughout the second half of the 20th century [26, 32, 51].

For propagation in isotropic media with magnetoelectric coupling (known as bi-isotropic media), all the material parameters presented in (2.1) can be represented by scalars, and the coupling coefficients take the form

$$\begin{aligned} \zeta &= \kappa^{\mathrm{nr}} + \kappa^{\mathrm{or}} + i\kappa^{\mathrm{er}}, \\ \xi &= \kappa^{\mathrm{nr}} + \kappa^{\mathrm{or}} - i\kappa^{\mathrm{er}}. \end{aligned} \tag{2.2}$$

In these expressions, κ^{er} contains the chirality of the medium, and κ^{nr} contains the nonreciprocal magnetoelectric effect, also known as the Tellegen parameter. More generally, κ^{nr} describes coupling due to many other nonreciprocal effects

including moving media and time-varying media [25]. In contrast, κ^{er} contains contributions from coupling mechanisms which are even in wavevector and reciprocal, hereafter referred to as even coupling. In addition to chirality, even coupling mechanisms common in metamaterials include substrate effects [35] and asymmetric microstructures such as split-ring resonators and Ω-particles [34]. The third parameter contributing to coupling, κ^{or}, accounts for reciprocal effects which are odd in wavevector, hereafter referred to as odd coupling. κ^{or} was recently demonstrated to occur in periodic lattices and is due to the finite phase velocity over a unit cell and multiple scattering effects, *i.e.*, nonlocal effects, which will also be discussed in this work as mesoscale effects. A major result of these findings is that neglecting κ^{or} in the homogenization of periodic arrays can result in effective properties that do not satisfy the restrictions imposed by passivity and causality on the response of a material when subjected to external fields [15, 23]. It is important to keep in mind that while κ^{nr}, κ^{or}, and κ^{er} are represented as scalars for the isotropic representation provided in Equation (2.2), the various effects just discussed may contribute to symmetric and/or asymmetric terms of the general bianisotropy tensors, $\underline{\boldsymbol{\xi}}$ and $\underline{\boldsymbol{\zeta}}$, in Equation (2.1) [51].

As mentioned above, asymmetric microstructures can lead to bi(an)-isotropy at the macroscale in electromagnetic metamaterials. Since this is shown to have an acoustic analog in the following section, it is informative to introduce an example electromagnetic response at the microscale that leads to coupled field behavior. One such structure is the so-called Ω-particle [34],

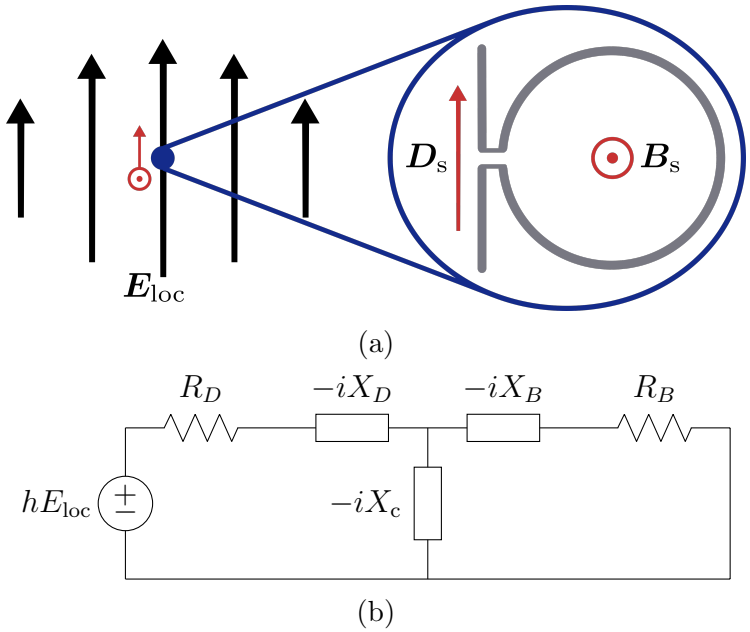

Figure 2.1: Ω-particle demonstrating a microscopic origin of even coupling κ^{er} in electromagnetism. (a) A perfectly conducting Ω-particle with height h produces electric $\boldsymbol{D}_\mathrm{s}$ and magnetic $\boldsymbol{B}_\mathrm{s}$ dipole scattering when located at a local electric field $\boldsymbol{E}_\mathrm{loc}$ maximum and magnetic field null. (b) The operation of the Ω-particle may be explained by its equivalent circuit [52, 53], where the response of the arms are modeled with reactance X_D, the response of the loop by X_B, and the coupling between the arms and loop by X_c. The resistances represent the scattered fields by the electric R_D and magnetic R_B dipoles due to the excitation by the local electric field and current around the loop.

which is illustrated in Figure 2.1a and described here. Given a perfectly conducting, Ω-shaped microstructure located at a local electric field $\boldsymbol{E}_\mathrm{loc}$ maximum and magnetic field null, the microscopic particle responds like the RLC circuit shown in Figure 2.1b, where the reactances X_D, X_B, and X_c are provided in References [52, 53]. The local electric field induces a charge separation, or a voltage source hE_loc, in the arms of the Ω particle that respond

as a perfeclty conducting rod of length h modeled by X_D. The charge separation in turn results in a current around the loop, which may be modeled by X_B, and X_c models the coupling between the arms and loop. Energy is dissipated through re-radiation in the form of a scattered electric dipole $\boldsymbol{D}_\mathrm{s}$ along the arms and a scattered magnetic dipole $\boldsymbol{B}_\mathrm{s}$ through the loop due to the time-varying current. These two forms of radiation are represented by red vectors in Figure 2.1a and as the resistances R_D and R_B in Figure 2.1b. In this manner, a microscopic particle may have a magnetic response to an electrical stimulus or an electric response due to a magnetic stimulus, *i.e.*, the Ω-particle may be also excited by a local magnetic field through the loop. Because this microstructure partially converts a stimulus of potential (kinetic) energy to a kinetic (potential) response, an inhomogeneous medium composed of many such subwavelegnth microstructures embedded in a background medium will exhibit macroscopic field coupling represented by constitutive relations in the form of Equation (2.1) [34].

In electromagnetism, materials are characterized by their electric and magnetic responses, which are coupled in the case of bianisotropic media. The analogous responses in elastodymanics correspond to relations between stress and strain and between velocity and momentum. In the following, a new class of materials known as Willis solids will be discussed, which are analagous to bianisotropic media due to coupling between stress-strain and momentum-velocity relations [30].

2.2 Bianisotropy in elastodynamics and acoustics

While bianisotropy was well known and in many ways a companion topic to metamaterials in electromagnetism since the beginning [51, 54], bianisotropy in elastodymnics and acoustics has just began to receive attention as a result of metamaterials; although, the analogs were observed several decades earlier. In the 1960s, several groups independently proposed that "acoustical activity" (analog to optical activity) would exist in non-centrosymmetric crystals [55–58]. This effect was measured in α quartz by Pine in 1970 [59], and acoustic chirality was later proposed and demonstrated in engineered composites in the 1980s [32, 33]. Chirality, which requires that the medium support transverse wave propagation with rotationally polarized fields, can only occur in elastic media and will be absent in fluids, which only support longitudinal motion. In mechanics, the term chirality also often refers to the related static effect whereby a uniform strain results in a torque, and chiral geometries can be used to achieve a negative Poisson's ratio [60]. Additionally, chiral elements have recently been used as spiral phase plates to produce acoustic orbital momentum [61], in which case the emergent acoustic beam from the plate has an azimuthal dependence, but the wave motion is still longitudinal.

Apart from the studies of chirality, J. R. Willis demonstrated in the 1980s that field coupling is a general result of dynamic homogenization of inhomogeneous media [27–29]. A surprising result of Willis' work was the prediction of coupled constitutive relations in the form of Equation (2.3) for both transverse and longitudinal waves, regardless if media supports rotational fields

[30, 36]. This coupling—a result of dynamic homogenization—has therefore come to be referred to as Willis coupling. Given that fluids only support longitudinal waves, one must therefore conclude that the analog of bianisotropy exists in fluid acoustics via Willis coupling. Recent work by Milton and Willis [30] outline the development of Willis' theory, and a recent review by Srivastava [31] highlights much of the work thus far in this area. The so-called Willis (bianisotropic) constitutive relations are generally presented in the form

$$\begin{aligned} \sigma_{ij} &= C_{ijkl}\varepsilon_{kl} + S_{ijk}\dot{\xi}_k, \\ \mu_i &= \tilde{S}_{ijk}\varepsilon_{jk} + \rho_{ij}\dot{\xi}_j, \end{aligned} \tag{2.3}$$

where the Cauchy stress tensor $\underline{\boldsymbol{\sigma}}$ is proportional to not only the infinitesimal strain tensor $\underline{\boldsymbol{\varepsilon}}$ via the fourth order stiffness tensor C but also to the time derivative of the displacement vector $\dot{\boldsymbol{\xi}}$ via a third order coupling tensor $\mathcal{S}$. Similarly, the momentum density vector $\boldsymbol{\mu}$ is also proportional to the strain via a third order coupling tensor $\tilde{\mathcal{S}}$ and the time derivative of the displacement vector via the mass-density tensor $\underline{\boldsymbol{\rho}}$ [30]. The general result provided by Willis was that dynamic homogenization leads to coupled constitutive relations with material properties that are temporally and spatially dispersive [16, 30]. Recent work by Nassar *et al.* [38] provides a detailed account of the necessary conditions for the application of Willis' homogenization theory to periodic media.

For 1D propagation, the constitutive parameters C, $\mathcal{S}$, $\tilde{\mathcal{S}}$, and $\underline{\boldsymbol{\rho}}$ reduce to scalars, C, S, $\tilde{S}$, and ρ, and for periodic media that are lossless and reciprocal, the coupling coefficients have been shown to be related by $\tilde{S} = -\text{conj}(S)$

for purely longitudinal propagation [37], purely shear propagation [17], and discrete systems [38]. This relation for lossless 1D mechanical systems is consistent with the relation between the even and odd reciprocal coupling parameters, κ^{er} and κ^{or}, in Equation (2.2). Additionally, Nemat-Nasser and Srivastava [37] noted that $\mathrm{Im}(S)$ is only non-zero when the unit cell is asymmetric and that $\mathrm{Re}(S)$ is finite (except in the static limit) regardless of unit cell symmetry. It has recently been demonstrated that $\mathrm{Re}(S)$ in lossless composites is due to nonlocal effects and has been shown to exist in periodic media with symmetric unit cells in 1D [40] and 2D [41] for acoustics and in 2D [19] for elastic waves. The work presented here demonstrates that for lossless composites $\mathrm{Im}(S)$ is due to asymmetric microstructures (even coupling) and $\mathrm{Re}(S)$ is the result of mesoscale effects associated with the finite phase velocity across the unit cell and multiple scattering in the lattice (odd coupling). It should be noted that constitutive relations in references may be in a complementary form compared to Equation (2.3), which will result in slightly different expressions for C, $\mathcal{S}$, $\tilde{\mathcal{S}}$, and $\underline{\boldsymbol{\rho}}$.

Independent of the works discussing Willis coupling, Koo *et al.* [39] recently demonstrated numerically and experimentally the use of acoustic bianisotropy to impedance match waveguides with different cross-sectional areas and to independently control reflection and transmission angles from a metasurface with a normally incident plane wave. Their demonstrations provide the first experimental evidence of acoustic bianisotropy and were inspired by the analogs to bianisotropy in electromagnetism. The experimental demon-

strations were recently explained in terms of Willis coupling by Muhlestein *et al.* [47] who provided detailed theoretical and experimental evidence of Willis coupling in a small asymmetric metamaterial sample. Also independently, Shui *et al.* [43] demonstrated nonreciprocal coupling for elastic waves using a layered medium with time-varying properties, which appears to be analogous to nonreciprocal coupling κ^{nr} in electromagnetism, though it was not described in this manner. A similar effect was recently discussed by Nassar *et al.* [44] who explained the effect as nonreciprocal Willis coupling.

The analogous coupled constitutive relations in fluid acoustics take the form

$$\begin{aligned} \boldsymbol{\mu} &= \underline{\boldsymbol{\rho}} \cdot \boldsymbol{u} - \boldsymbol{\eta} p, \\ \varepsilon &= \boldsymbol{\gamma} \cdot \boldsymbol{u} - \beta p, \end{aligned} \tag{2.4}$$

where vector fields are momentum density $\boldsymbol{\mu}$ and acoustic particle velocity $\boldsymbol{u}$, and scalar fields are volume strain ε and acoustic pressure p. The fields are related by the anisotropic mass density $\underline{\boldsymbol{\rho}}$, adiabatic compressibility β, and coupling vectors $\boldsymbol{\eta}$ and $\boldsymbol{\gamma}$. Consistent with the origins of bianisotropy in electromagnetism as presented in Equation (2.2) and the observation in lossless 1D elastodynamic studies that $\tilde{S} = -\mathrm{conj}(S)$ [17, 37, 38], the work presented here demonstrates in Chapter 3 that for passive, reciprocal fluids

$$\begin{aligned} \boldsymbol{\eta} &= \boldsymbol{\chi}^{\mathrm{o}} + i\boldsymbol{\chi}^{\mathrm{e}}, \\ \boldsymbol{\gamma} &= \boldsymbol{\chi}^{\mathrm{o}} - i\boldsymbol{\chi}^{\mathrm{e}}, \end{aligned} \tag{2.5}$$

where $\boldsymbol{\chi}^{\mathrm{o}}$ is odd coupling, *i.e.*, odd in wavevector $\boldsymbol{k}$ such that $\boldsymbol{\chi}^{\mathrm{o}}(\boldsymbol{k}) = -\boldsymbol{\chi}^{\mathrm{o}}(-\boldsymbol{k})$, and $\boldsymbol{\chi}^{\mathrm{e}}$ is even coupling, *i.e.*, even in wavevector $\boldsymbol{k}$ such that $\boldsymbol{\chi}^{\mathrm{e}}(\boldsymbol{k}) = \boldsymbol{\chi}^{\mathrm{e}}(-\boldsymbol{k})$.

As discussed in the previous section, coupling in electromagnetism occurs between electric and magnetic material responses, two distinct phenomena. The origins of coupling in acoustics and elastodynamics are not as obvious because all the fields are thermodynamic in nature; however, the origins become more evident upon inspection of the acoustic constitutive relations, Equation (2.4). In the absence of coupling, *i.e.*, $\boldsymbol{\gamma} = \boldsymbol{\eta} = 0$, the first expression in Equation (2.4) is simply the definition of momentum, a vector equation representing purely translational motion at a vanishingly small material point. The velocity and momentum density at this field point are related to the local kinetic energy. A particle demonstrating this type of motion is associated with acoustic dipolar radiation and is therefore often referred to as a dipole. Similarly, in the absence of coupling, the second expression in Equation (2.4) is a Hookean relation and the equation of state for an isentropic fluid, which is a scalar equation representing purely compressional motion at a vanishingly small material point. The pressure and volume strain at this field point are related to the local potential energy. A particle demonstrating this type of motion is associated with acoustic monopolar radiation and is therefore often referred to as a monopole. It is the coupling between monopolar and dipolar motion at the microscale and/or mesoscale of inhomogeneous fluids that leads to macroscopic Willis, or bianisotopic, constitutive relations in effective fluids.

In the previous section, the microscopic asymmetry present in an inhomogeneous medium consisting of Ω-particles leads to macroscale coupling due to the coupled scattering of the inhomogeneity. An analogous asymmet-

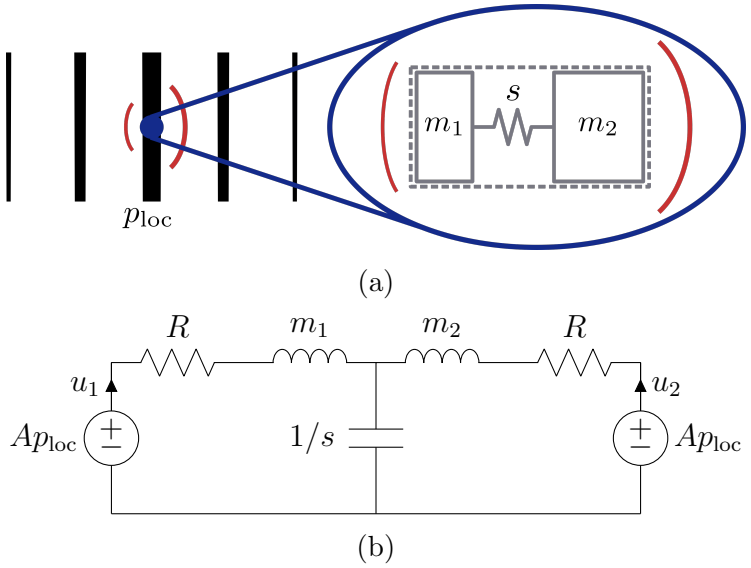

Figure 2.2: Asymmetric acoustic inhomogeneity demonstrating the microscopic origin of even coupling. (a) Inhomogeneity with cross-sectional area A consisting of two masses m_1 and m_2 separated by a spring with stiffness s and located at a local acoustic pressure maximum and particle velocity null. (b) Equivalent circuit model demonstrating that the local pressure acts as force sources Ap_{loc} in series with the masses m_1 and m_2, separated by the compliance $1/s$. The resistors R represent the scattered acoustic field due to the motion of the masses. For $m_1 \neq m_2$, $u_1 \neq u_2$ implying that the inhomogeneity response is not purely monopolar despite the monopole nature of the source. Thus, the scattered wave will contain monopole and dipole components.

ric acoustic inhomogeniety and equivalent circuit are presented in Figure 2.2. Consider a microscopic inhomogenity with cross-sectional area A consisting of two masses m_1 and m_2 separated by an ideal spring with stiffness s and located at a local acoustic pressure maximum and particle velocity null as shown in Figure 2.2a. Scattered acoustic waves, represented by red curves, will radiate from both masses. Since a pressure maximum coincides with a particle velocity null, *i.e.*, $\boldsymbol{u}_{\text{loc}} = 0$, then the local field imposes a purely monopole ex-

citation. The monopolar excitation is indicated by force sources in series with the masses and in parallel with the compliance $1/s$ as shown in the equivalent circuit in Figure 2.2b. In the equivalent circuit, the velocities of the masses are labeled as u_1 and u_2, which are positive for the masses moving towards each other with positive pressure, and the resistances R represent the acoustic field radiated into the background fluid from the motion of the masses. Purely monopolar motion of the inhomogeneity requires $u_1 = u_2$, and purely dipolar motion of the inhomogeneity requires $u_1 = -u_2$. From the equivalent circuit, for a monopole excitation and $m_1 \neq m_2$, the inhomogeneity must respond to combination of monopolar and dipolar motion, because $u_1 \neq u_2$ and also $u_1 \neq -u_2$. This simple model clearly indicates the origins of even coupling at the microscale due to the presence of asymmetric microscopic inhomogeneities. An inhomogeneous medium consisting of many such microstructures will exhibit some amount of coupling in effective parameters as in Equations (2.3) and (2.4).

While even coupling can originate from asymmetry at the microscale, odd coupling arises at the mesoscale. For example, consider an array of inhomogeneities with feature size l and periodicity L in a background fluid with wavenumber $k_0 = \omega/c_0 = 2\pi/\lambda_0$. Dispersion of the acoustic waves propagating in this array can be described with the macroscopic wavenumber $k = \omega/c = 2\pi/\lambda$. Even though the inhomogeneity may indeed be small compared to the wavelength in the background media, the phase change over a unit cell may be significant due to resonances, *i.e.*, even though $k_0 l < 0.1$

in many cases $kL > 1$, which is often the case for metamaterials with $c \to 0$ because for $c \to 0$ then $\lambda \to 0$ at finite frequency. The finite phase change over the distance of a unit cell, *i.e.*, $kL > 0$, demonstrates that there is an exchange between kinetic and potential energy due to effective wave propagation over the finite unit cell. In the macroscopic constitutive relations, the phase change leads to odd coupling; odd because the phase change over the unit cell will change sign with the opposite propagation direction. This provides a qualitative argument for considering odd coupling, which quantifies the exchange between monopolar and dipole motion due to finite phase change over the length of the unit cell. Odd coupling becomes particularly profound in slow phase speed metamaterials, because as c tends to zero so does the macroscopic wavelength, and when λ becomes comparable to L, the macroscopic description of the inhomogeneous medium as a single homogeneous material with effective properties begins to lose physical meaning. The mesoscopic origins of odd coupling are demonstrated in the homogenization procedure derived in Chapter 4, and the impact of neglecting odd coupling in 1D examples is discussed in Chapter 5.

This chapter has provided an overview and simple examples illustrating the physical basis for bianisotropy in electromagnetism, elastodynamics and acoustics. The next chapter considers the physical restrictions on the macroscopic parameters of a bianisotropic acoustic fluid which are of fundamental importance for assessing the applicability of dynamic homogenization models used to describe acoustic metamamterials.

Chapter 3

Physical Restrictions on Macroscopic Material Properties

3.1 Motivations and overview

The Ashby chart in Figure 1.1 illustrates the extreme effects achievable if ρ and κ can be accurately controlled. One area that has received much attention is the negative phase speed [10, 11], which requires that subwavelength dynamics result in simultaneous effective dynamic density and bulk modulus being less than zero. More specifically, $\mathrm{Re}(\rho) < 0$ and $\mathrm{Re}(\kappa) < 0$, where the real part is specified because frequency dependent lossy media is often modeled with complex properties. For convenience, these lossy material properties can be expressed in polar notation as $\rho = |\rho|e^{i\theta_\rho}$ and $\kappa = |\kappa|e^{i\theta_\kappa}$ [62]. In the polar notation, the phase speed is given by

$$c = \left(\frac{|\kappa|}{|\rho|}\right)^{1/2} e^{i(\theta_\kappa - \theta_\rho)/2} \tag{3.1}$$

In order to have a negative phase speed in a lossless metamaterial, $\theta_\rho = \pm\pi$ and $\theta_\kappa = \mp\pi$. Alternatively, one can express phase speed in terms of compressibility $\beta = \kappa^{-1}$, then

$$c = (|\rho||\beta|)^{-1/2} e^{-i\left(\theta_\rho + \theta_\beta\right)/2}. \tag{3.2}$$

For $\mathrm{Re}(c) < 0$, $\theta_\rho = \theta_\beta = \pm\pi$. Equations (3.1) and (3.2) demonstrate that it is not just a matter of having negative properties; additionally, the phase angles of these properties must be related in a particular way for the fluid to exhibit negative phase speed. For the case of lossless fluids, two possible phase angle combinations exist.

Recent works in elastodynamics [24, 63, 64], suggest that only one of the choices of phase angle will satisfy passivity, which is consistent with restrictions on electromagnetic properties [23]. However, many studies suggest that as long as the imaginary part of the wavenumber has the correct sign such that an advancing wave attenuates then the model is acceptable [18, 62, 65, 66], *i.e.*, using the $e^{-i\omega t}$ time convention, a wave traveling in the $+\hat{x}$-direction should satisfy

$$\mathrm{Im}(k) = \omega \left(|\rho||\beta|\right)^{1/2} \sin\left(\frac{\theta_\rho + \theta_\beta}{2}\right) \geq 0. \tag{3.3}$$

However, this inequality only places a restriction on $\theta_\rho + \theta_\beta$, not on θ_ρ and θ_β individually [62].

The purpose of this chapter is to derive restrictions on the material parameters of bianisotropic acoustic fluids based on reciprocity, passivity, and causality. Since the previous chapters have only discussed material properties, Sec. 3.2 introduces the dynamic equations that are the foundation of linear acoustics. Restrictions based on reciprocity and passivity are drived in Sec. 3.3, and causal relations are discussed for relaxing and resonant media in Sec. 3.4. The derivations and discussions in this chapter follow the recent work of Muhlestein *et al.* [24].

3.2 Conventional linear acoustics

Acoustic wave propagation is described through the appropriate application of the Navier-Stokes equation (conservation of momentum), the continuity equation (conservation of mass), entropy equation (internal energy), and an equation of state (constitutive equation) [67]. For a linear, locally reacting fluid, the conservation of momentum expression simplifies to

$$\nabla \hat{p} = -\dot{\hat{\boldsymbol{\mu}}} + \hat{\boldsymbol{f}}. \tag{3.4}$$

In this time-domain expression (denoted by the carets over the variables), the scalar $\hat{p}$ represents the acoustic pressure; the vector $\hat{\boldsymbol{\mu}}$ is the momentum density; and the vector $\hat{\boldsymbol{f}}$ represents body forces, which can also be described as dipole sources, at the point of evaluation. The overdot represents the partial time-derivative operation. For non-dispersive fluids, the assumption that $\hat{\boldsymbol{\mu}} = \rho_0 \hat{\boldsymbol{u}}$ is often made *a priori*, where ρ_0 represents the static mass density of the fluid supporting the acoustic wave and $\hat{\boldsymbol{u}}$ represents the acoustic particle velocity.

The linearized form of the continuity equation is usually expressed as $\dot{\hat{\rho}} = \hat{q} - \rho_0 \nabla \cdot \hat{\boldsymbol{u}}$ [67], where $\hat{\rho}$ is the instantaneous mass density and $\hat{q}$ represents volume, or monopole, sources. An equivalent useful relationship for the continuity equation resulting from an analysis of strain rates was provided by Hunt [68], who showed that

$$\nabla \cdot \hat{\boldsymbol{u}} = \dot{\hat{\varepsilon}} + \hat{q}, \tag{3.5}$$

where $\hat{\varepsilon}$ is the volume strain (dilatation in [68]). For linear acoustics, volume strain is proportional to acoustic pressure via a Hookean relation $\hat{\varepsilon} = -\beta_0 \hat{p}$. Here, β_0 is the adiabatic compressibility of the fluid, which is the inverse of the bulk modulus. For the remainder of this work, compressibility is used rather than bulk modulus, because the compressibility form of the constitutive equations results in derivations being in terms of pressure and particle velocity as independent, which are the most commonly used field variables in acoustics [67]. Also, this form is most analogous to *E*-*H* electromagnetism [69], enabling useful comparisons with existing literature in that field.

Assuming an $e^{-i\omega t}$ time dependence, *i.e.*, $\hat{p} = \mathrm{Re}(pe^{-i\omega t})$, the expressions describing momentum and mass conservation become

$$\begin{aligned} \nabla p &= i\omega \boldsymbol{\mu} + \boldsymbol{f}, \\ \nabla \cdot \boldsymbol{u} &= -i\omega \varepsilon + q, \end{aligned} \tag{3.6}$$

where the time dependence has been suppressed. For the remainder of this chapter, the constitutive equations will be assumed to have the bianisotropic form as presented in Equation (2.4), *i.e.*,

$$\begin{aligned} \boldsymbol{\mu} &= \underline{\boldsymbol{\rho}} \cdot \boldsymbol{u} - \boldsymbol{\eta} p, \\ \varepsilon &= \boldsymbol{\gamma} \cdot \boldsymbol{u} - \beta p, \end{aligned} \tag{3.7}$$

which reduce to conventional anisotropic constitutive relations if $\boldsymbol{\eta} = \boldsymbol{\gamma} = 0$. This assumption facilitates the determination of physical restrictions on effective material properties due to reciprocity, passivity, and causality, which is central to the present work.

3.3 Reciprocity and passivity

If all of the constituents of an inhomogeneous medium are linear, reciprocal, and passive and no external fields are applied, then the effective medium response must also be represented by constants that are linear, passive, and reciprocal.

3.3.1 Reciprocity

As illustrated in Figure 3.1, reciprocity describes the symmetry of transmission between two points in space. To derive the reciprocity condition, consider the dynamic equations for two independent source distributions, indicated by the subscripts 1 and 2, expressed as

$$\begin{aligned} \nabla p_1 &= i\omega \boldsymbol{\mu}_1 + \boldsymbol{f}_1, \\ \nabla \cdot \boldsymbol{u}_1 &= -i\omega \varepsilon_1 + q_1, \end{aligned} \tag{3.8}$$

and

$$\begin{aligned} \nabla p_2 &= i\omega \boldsymbol{\mu}_2 + \boldsymbol{f}_2, \\ \nabla \cdot \boldsymbol{u}_2 &= -i\omega \varepsilon_2 + q_2. \end{aligned} \tag{3.9}$$

Taking the dot product of $\boldsymbol{u}_2$ and the first equation in (3.8) and adding it to the product of p_1 and the second equation in (3.9) yields

$$\begin{aligned} \boldsymbol{u}_2 \cdot \nabla p_1 + p_1 \nabla \cdot \boldsymbol{u}_2 &= \nabla \cdot (p_1 \boldsymbol{u}_2) \\ &= i\omega \left(\boldsymbol{u}_2 \cdot \boldsymbol{\mu}_1 - p_1 \varepsilon_2 \right) + \boldsymbol{u}_2 \cdot \boldsymbol{f}_1 + p_1 q_2. \end{aligned} \tag{3.10}$$

Similarly, taking the dot product of $\boldsymbol{u}_1$ and the first equation in (3.9) and adding it to the product of p_2 and the second equation in (3.8) yields

$$\begin{aligned} \boldsymbol{u}_1 \cdot \nabla p_2 + p_2 \nabla \cdot \boldsymbol{u}_1 &= \nabla \cdot (p_2 \boldsymbol{u}_1) \\ &= i\omega \left(\boldsymbol{u}_1 \cdot \boldsymbol{\mu}_2 - p_2 \varepsilon_1 \right) + \boldsymbol{u}_1 \cdot \boldsymbol{f}_2 + p_2 q_1. \end{aligned} \tag{3.11}$$

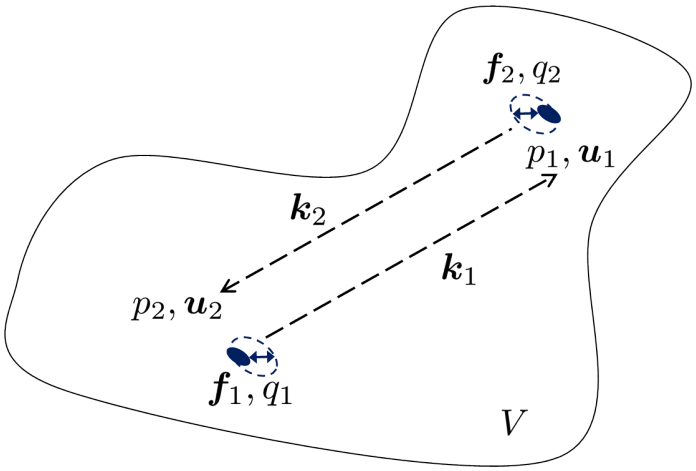

Figure 3.1: Geometry for reciprocity condition.

Subtracting (3.11) from (3.10) and integrating over a volume V enclosed by a surface A with outward normal $\hat{n}$ yields

$$\int_A (p_1 \boldsymbol{u}_2 - p_2 \boldsymbol{u}_1) \cdot \hat{n} dA = \int_V (\boldsymbol{u}_2 \cdot \boldsymbol{f}_1 - \boldsymbol{u}_1 \cdot \boldsymbol{f}_2 + p_1 q_2 - p_2 q_1)\, dV - i\omega \int_V (\boldsymbol{u}_1 \cdot \boldsymbol{\mu}_2 - \boldsymbol{u}_2 \cdot \boldsymbol{\mu}_1 + p_1 \varepsilon_2 - p_2 \varepsilon_1)\, dV. \tag{3.12}$$

Now, taking the surface A to infinity and assuming no waves approach from infinity, the integral on the left hand side of (3.12) must be zero because the fields must go to zero at infinity by the Sommerfeld radiation condition [70]. The first integral on the right hand side of (3.12) expresses the exchange of source and receiver locations. For a reciprocal fluid, this integral must be zero by the Rayleigh reciprocity theorem [71]. Therefore, a reciprocal fluid must satisfy

$$\int_V (\boldsymbol{u}_1 \cdot \boldsymbol{\mu}_2 - \boldsymbol{u}_2 \cdot \boldsymbol{\mu}_1 + p_1 \varepsilon_2 - p_2 \varepsilon_1)\, dV = 0 \tag{3.13}$$

at every point, which requires that the integrand be zero.

In Chapter 2, it is discussed that reciprocal coupling vectors may contain components that are even and odd in wavevector $\boldsymbol{k}$, *i.e.*, $\boldsymbol{\eta} = \boldsymbol{\eta}^{\mathrm{e}} + \boldsymbol{\eta}^{\mathrm{o}}$ and $\boldsymbol{\gamma} = \boldsymbol{\gamma}^{\mathrm{e}} + \boldsymbol{\gamma}^{\mathrm{o}}$. For the exchange of source and receiver, $\boldsymbol{k}_1 = -\boldsymbol{k}_2$. Now, substituting Equation (3.7) into Equation (3.13) leads to

$$\begin{aligned} \boldsymbol{u}_1 \cdot \left(\underline{\boldsymbol{\rho}} - \underline{\boldsymbol{\rho}}^{\mathrm{T}}\right) \cdot \boldsymbol{u}_2 + (\boldsymbol{\eta}^{\mathrm{e}} + \boldsymbol{\gamma}^{\mathrm{e}}) \cdot (p_1 \boldsymbol{u}_2 - p_2 \boldsymbol{u}_1) \\ + (\boldsymbol{\eta}^{\mathrm{o}} - \boldsymbol{\gamma}^{\mathrm{o}}) \cdot (p_1 \boldsymbol{u}_2 + p_2 \boldsymbol{u}_1) = 0. \end{aligned} \tag{3.14}$$

Therefore, the bianisotropic constitutive parameters for a reciprocal fluid must satisfy $\underline{\boldsymbol{\rho}} = \underline{\boldsymbol{\rho}}^{\mathrm{T}}$, where the superscript T denotes transpose, $\boldsymbol{\eta}^{\mathrm{o}} = \boldsymbol{\gamma}^{\mathrm{o}}$, and $\boldsymbol{\eta}^{\mathrm{e}} = -\boldsymbol{\gamma}^{\mathrm{e}}$, which suggests that $\boldsymbol{\gamma} = \boldsymbol{\eta}^{\mathrm{o}} - \boldsymbol{\eta}^{\mathrm{e}}$.

3.3.2 Passivity

A passive media is one that does not provide energy to field [24, 72]. The time-averaged acoustic intensity (sometimes referred to as the acoustic Poynting vector) is given by

$$\boldsymbol{I} = \frac{1}{2} p \boldsymbol{u}^* = \frac{1}{2} p^* \boldsymbol{u}, \tag{3.15}$$

where superscript * denotes complex conjugate [67]. The real part of the intensity vector $\boldsymbol{I}$ represents the directed average power flow density of the acoustic field, and the origin of this flow may be obtained by taking its divergence. Since $\mathrm{Re}(\nabla \cdot \boldsymbol{I})$ is the rate of energy generated at a point, then for a passive media $\mathrm{Re}(\nabla \cdot \boldsymbol{I}) \leq 0$, where equality is the lossless case [72].

In the absence of sources, substituting the dynamic equations, Equation (3.6), and the constitutive relations, Equation (3.7), into the divergence of

Equation (3.15) yields

$$\begin{aligned}
-\mathrm{Re}\left(\nabla\cdot\boldsymbol{I}\right) &= -\frac{1}{2}\mathrm{Re}\left(i\omega\boldsymbol{\mu}\cdot\boldsymbol{u}^{*}+i\omega\varepsilon^{*}p\right)\\
&= -\frac{i\omega}{4}\left(\boldsymbol{\mu}\cdot\boldsymbol{u}^{*}-\boldsymbol{\mu}^{*}\cdot\boldsymbol{u}+\varepsilon^{*}p-\varepsilon p^{*}\right)\\
&= -\frac{i\omega}{4}\left[\boldsymbol{u}^{*}\cdot\left(\underline{\boldsymbol{\rho}}-\underline{\boldsymbol{\rho}}^{*\mathrm{T}}\right)\cdot\boldsymbol{u}+2i\mathrm{Im}\left(\beta\right)|p|^{2}\right.\\
&\qquad\left.-\left(\boldsymbol{\eta}-\boldsymbol{\gamma}^{*}\right)\cdot p\boldsymbol{u}^{*}+\left(\boldsymbol{\eta}^{*}-\boldsymbol{\gamma}\right)\cdot p^{*}\boldsymbol{u}\right]\geq 0.
\end{aligned}\tag{3.16}$$

This expression provides the rate at which energy is dissipated by the fluid at a point in terms of the fluid parameters. Therefore, the constitutive parameters of a *lossless* bianisotropic fluid must satisfy $\underline{\boldsymbol{\rho}}=\underline{\boldsymbol{\rho}}^{*\mathrm{T}}$, $\mathrm{Im}\left(\beta\right)=0$, and $\boldsymbol{\eta}=\boldsymbol{\gamma}^{*}$.

3.3.3 Reciprocal and passive fluids

Restrictions on a bianisotropic fluid that satisfies both reciprocity and passivity are determined by substituting the results of Equation (3.14) into Equation (3.16). After some rearranging,

$$\begin{aligned}
&\frac{\omega}{2}\boldsymbol{u}^{*}\cdot\mathrm{Im}\left(\underline{\boldsymbol{\rho}}\right)\cdot\boldsymbol{u}+\frac{\omega}{2}\mathrm{Im}\left(\beta\right)|p|^{2}\\
&\qquad-\omega\mathrm{Im}\left(\boldsymbol{\eta}^{\mathrm{o}}\right)\cdot\mathrm{Re}\left(p\boldsymbol{u}^{*}\right)-\omega\mathrm{Re}\left(\boldsymbol{\eta}^{\mathrm{e}}\right)\cdot\mathrm{Im}\left(p\boldsymbol{u}^{*}\right)\geq 0.
\end{aligned}\tag{3.17}$$

Defining $\boldsymbol{\eta}^{\mathrm{e}}=i\boldsymbol{\chi}^{\mathrm{e}}$ and $\boldsymbol{\eta}^{\mathrm{o}}=\boldsymbol{\chi}^{\mathrm{o}}$, Equation (3.17) becomes

$$\begin{aligned}
&\frac{\omega}{2}\boldsymbol{u}^{*}\cdot\mathrm{Im}\left(\underline{\boldsymbol{\rho}}\right)\cdot\boldsymbol{u}+\frac{\omega}{2}\mathrm{Im}\left(\beta\right)|p|^{2}\\
&\qquad-\omega\mathrm{Im}\left(\boldsymbol{\chi}^{\mathrm{o}}\right)\cdot\mathrm{Re}\left(p\boldsymbol{u}^{*}\right)+\omega\mathrm{Im}\left(\boldsymbol{\chi}^{\mathrm{e}}\right)\cdot\mathrm{Im}\left(p\boldsymbol{u}^{*}\right)\geq 0.
\end{aligned}\tag{3.18}$$

Now, all the restrictions on the bianisotropic material properties due to reciprocity and passivity are placed on the imaginary parts. In order for the fluid to be reciprocal and passive, the inequality must hold at any point where either $\boldsymbol{u}=0$ or $p=0$. Therefore, $\mathrm{Im}\left(\underline{\boldsymbol{\rho}}\right)\geq 0$, $\mathrm{Im}\left(\beta\right)\geq 0$, and $\mathrm{Im}\left(\boldsymbol{\chi}^{\mathrm{o}}\right)$ and $\mathrm{Im}\left(\boldsymbol{\chi}^{\mathrm{e}}\right)$

are bounded. Nothing can be said about the signs of $\mathrm{Im}\,(\boldsymbol{\chi}^{\mathrm{o}})$ and $\mathrm{Im}\,(\boldsymbol{\chi}^{\mathrm{e}})$, because the real and imaginary parts of $p\boldsymbol{u}^*$ change sign with direction. For lossless fluids, the imaginary parts of all parameters are zero.

3.4 Causality

Causality refers to the physical principle that a response may not precede an excitation. While causality is guaranteed for linear passive media [73], considering it separately provides insight into dynamic behavior of parameters within certain frequency bands of interest. The analysis of this section will apply directly to density and compressibility but not to the coupling parameters in the form presented here, because $\boldsymbol{\chi}^{\mathrm{e}}$ and $\boldsymbol{\chi}^{\mathrm{o}}$ hide temporal and spatial derivatives [24]. The presence of derivatives in the coupling parameters is discussed in Sec. 5.1.3.

A real, time domain response function $\hat{A}(t)$ has a frequency domain representation which can be separated in real and imaginary parts, *i.e.*, $A(\omega) = A'(\omega) + iA''(\omega)$, where $-\infty < \omega < \infty$ in general. Since $A(\omega)$ may represent ρ or β, the results of the previous section suggest that $A''(\omega)$ will be related to loss and that $A''(\omega) \geq 0$. The Hilbert transform pairs (derived in References [24] and [50]) explicitly relate $A''(\omega)$ to $A'(\omega) - A'(\infty)$,

$$\begin{aligned} A'(\omega) - A'(\infty) &= \frac{2}{\pi}\mathcal{P}\int_0^\infty \frac{\lambda A''(\lambda)}{\lambda^2 - \omega^2} d\lambda \\ A''(\omega) &= -\frac{2}{\pi}\mathcal{P}\int_0^\infty \frac{\omega A'(\lambda)}{\lambda^2 - \omega^2} d\lambda, \end{aligned} \tag{3.19}$$

where $A'(\infty)$ is the "frozen state" response (*i.e.*, when all relaxation processes

are much slower than the driving frequency), $\mathcal{P}$ denotes that the principle value of the integral be taken, and symmetries have been exploited to reduced the range of integration to $0 \leq \omega < \infty$ [24]. These relations are also known as the Kramers-Krönig relations and are exact in theory, but often in practice, the integrals can only be approximated numerically for a finite frequency range [24]. However, Equation (3.19) provides insight into expected dispersion for limited frequency bands in which $A''(\omega) \ll A'(\omega)$ and in which the contribution to the infinite integrals at $\lambda = \omega$ is either dominant or negligible.

The case in which $\lambda = \omega$ provides the dominant contribution to the integrals in Equation (3.19) was explored by O'Donnell *et al.* in order to better predict the properties of relaxing (viscoelastic) acoustic media at ultrasonic frequencies [74]. By using a change of variables and expanding about $\lambda = \omega$ in the integrand of the second expression of Equation (3.19), they demonstrated that the imaginary part of the relaxation function can be related to the rate of change of the real part with respect to the frequency (*i.e.*, the spectral derivative) evaluated at the frequency of interest by the approximation

$$A''(\omega) \approx -\frac{\pi}{2}\omega\frac{\partial A'}{\partial \omega}. \tag{3.20}$$

Since $A'' \geq 0$ for media satisfying passivity and reciprocity, the real part of density and compressibility must decrease with increasing frequency in bands for which relaxation dominates.

The second case in which loss is negligible at the frequency of interest was considered by Landau and Lifshitz and is often used in electromagnetism

[50]. Because $A''(\omega) \approx 0$, the integrand at $\lambda = \omega$ has a negligible contribution to the total integration compared to frequencies at which A'' may become very large, such as at frequencies where microstructural resonances occur or the boundaries of stopbands due to mesoscopic interaction. In this case, it is not necessary to take principle value of the integral in the first expression in Equation (3.19), because the point $\lambda = \omega$ no longer lies in the region of integration. The expression can therefore be differentiated with respect to ω to yield

$$\frac{\partial A'}{\partial \omega} = \frac{4}{\pi} \int_0^\infty \frac{\lambda\omega}{\left(\lambda^2 - \omega^2\right)^2} A''(\lambda) d\lambda, \tag{3.21}$$

and because the integrand must be positive, Equation (3.21) suggests that A' must have a positive slope in fluids with negligible loss and resonant microstructure, as opposed to the negative slope in relaxing fluids, Equation 3.20.

This discrepancy is important to understand since natural fluids follow the relaxing media approximation, but acoustic metamaterials are often composed of low loss materials with resonant microstructures. Therefore, away from resonances and stopbands, acoustic metamaterial parameters should follow Landau and Lifshitz's analysis. A qualitative comparison of these two effects is presented in Figure 3.2. In the figure, relaxation is observed at lower frequencies, and in this region (shaded red), the finite imaginary part leads to a decreasing real part of A. Beyond the relaxation region, the large peak in the imaginary part at the resonance dominates the integral, and on either side of the resonance (shaded blue) the real part of A has a positive slope. Neither

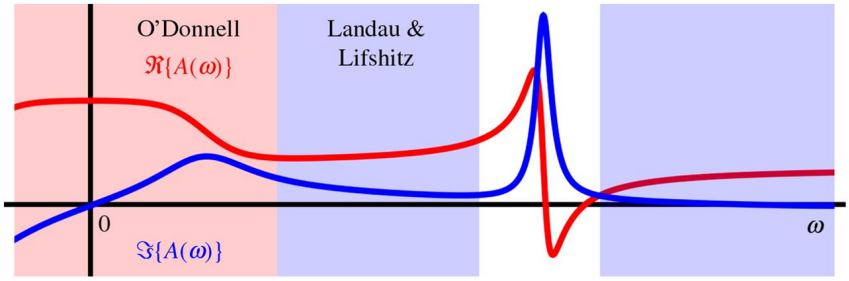

Figure 3.2: Example complex function $A(\omega)$ highlighting approximate regions of applicability of the dispersion simplifications by O'Donnell *et al.* [74] and by Landau and Lifshitz [50]. Adapted with permission from Reference [24].

of the two approximations are sufficient to predict behavior at frequencies near to the resonance.

3.5 Summary of results for 1D metamaterials

For 1D studies, restrictions may be simplified further since the density and coupling parameters reduce to scalars. Equation (3.18) therefore becomes

$$\begin{aligned}\frac{\omega}{2}\mathrm{Im}\left(\rho\right)|u|^2+\frac{\omega}{2}\mathrm{Im}\left(\beta\right)|p|^2-\frac{\omega}{2}\left[\mathrm{Im}\left(\chi^{\mathrm{o}}\right)+i\mathrm{Im}\left(\chi^{\mathrm{e}}\right)\right]pu^*\\-\frac{\omega}{2}\left[\mathrm{Im}\left(\chi^{\mathrm{o}}\right)-i\mathrm{Im}\left(\chi^{\mathrm{e}}\right)\right]p^*u\geq 0,\end{aligned}\tag{3.22}$$

which can be cast into matrix form as

$$\frac{\omega}{2}\begin{bmatrix}u & p\end{bmatrix}\cdot\begin{bmatrix}\mathrm{Im}\left(\rho\right) & -\mathrm{Im}\left(\chi^{\mathrm{o}}\right)+i\mathrm{Im}\left(\chi^{\mathrm{e}}\right)\\-\mathrm{Im}\left(\chi^{\mathrm{o}}\right)-i\mathrm{Im}\left(\chi^{\mathrm{e}}\right) & \mathrm{Im}\left(\beta\right)\end{bmatrix}\cdot\begin{bmatrix}u\\p\end{bmatrix}^*\geq 0.\tag{3.23}$$

In order to satisfy the inequality, the parameters matrix must be positive definite, which requires that its trace and determinant be positive [72]. Therefore,

reciprocal, passive, resonant, 1D acoustic metamaterials must satisfy

$$\begin{aligned} \mathrm{Im}\,(\rho) &\geq 0, \\ \mathrm{Im}\,(\beta) &\geq 0, \\ \mathrm{Im}\,(\rho)\,\mathrm{Im}\,(\beta) &\geq \left[\mathrm{Im}\,(\chi^{\mathrm{o}})\right]^2 + \left[\mathrm{Im}\,(\chi^{\mathrm{e}})\right]^2, \\ \partial\rho/\partial\omega &\geq 0, \\ \partial\beta/\partial\omega &\geq 0, \end{aligned} \tag{3.24}$$

where the last two expressions are valid away from resonances and bandgaps, and all imaginary parts are equal to zero in lossless fluids.

Restrictions on the material parameters of bianisotropic acoustic fluids based on reciprocity, passivity, and causality are derived in the preceding sections of this chapter. The reason for including these derivations is to set limitations for the effective metamaterial properties one can expect to observe from a homogenization scheme or from material properties extracted from experimental measurements. These restrictions will be used in in Chapter 5 to address why metamaterial parameters in many published works do not to satisfy these restrictions.

Chapter 4

Source-Driven Homogenization

This chapter outlines a source-driven homogenization theory based on multiple scattering and modeled after analogous work in electromagnetism [15]. It differs from previous acoustic multiple scattering homogenization approaches, *e.g.*, Twersky [75, 76] and Torrent and Sánchez-Dehesa [77] and references therein, by taking a source-driven approach and by allowing for coupling between monopole and dipole responses as discussed in Section 2.2. The source-driven approach is required to arrive at unique solutions for the effective material properties [14–16]. The homogenization procedure will be introduced as follows. In Section 4.1, equations for the conservation of momentum (3.4) and mass (3.5) will be used to determined microscopic (or exact) and macroscopic fields due to a source distribution with an $e^{i\boldsymbol{k}\cdot\boldsymbol{x}}e^{-i\omega t}$ dependence, with and without inhomogeneities. In Section 4.2, macroscopic effective fields will be related to the scattering properties of inhomogeneities. The dependency of macroscopic parameters on the scattering properties of the inhomogeneities will be referred to as the *microscopic* effects. The relation of macroscopic fields to *mesoscopic* effects resulting from finite phase velocity along the array of inhomogeneities and interaction between inhomogeneities due to multiple scattering will be introduced in Sections 4.1 and 4.3, respectively. The re-

sponses of the inhomogeneities, their long range interaction, and finite unit cell effects will be expressed in terms of monopole, dipole, and coupled coefficients. The homogenized, *effective* material parameters will be explicitly solved for in the cases of periodic arrays of identical inhomogeneities for 1-, 2-, and 3D space in Section 4.5. The procedure may be generalized to random arrays and the point of departure from general arrays to periodic arrays will be highlighted in Section 4.3.

4.1 Source-driven homogenization theory

Consider an homogeneous fluid characterized by mass density ρ_0 and adiabatic compressibility β_0 which contains an arbitrary, externally controlled distributions of sources. The acoustic pressure field that results from such a source distribution is shown in Figure 4.1a. The source distribution exists at every point and can be modeled with time-harmonic body forces (dipole sources) with strength $\boldsymbol{f}_{\text{ext}}$ and time-harmonic volume velocity (monopole sources) with strength q_{ext}. The source distribution imposes an arbitrary $e^{i\boldsymbol{k}\cdot\boldsymbol{x}}e^{-i\omega t}$ dependence in the background medium. Although fictitious in practice, a continuous source distribution guarantees uniqueness of fields and permits the ability to impose acoustic pressure and velocity fields with any desired $(\omega, \boldsymbol{k})$ pair, making it possible to uniquely determine the constitutive properties for any $(\omega, \boldsymbol{k})$ combination [14–16]. This is the basis of the so-called "source-driven" homogenization approach.

The inhomogeneous linear acoustic equations for conservation of mo-

(a) $p(\boldsymbol{x}) = p_{\text{ext}} e^{i\boldsymbol{k}\cdot\boldsymbol{x}}$

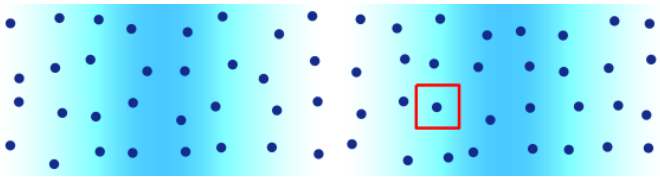

(b) $p(\boldsymbol{x}) = p_{\text{s}}(\boldsymbol{x}) + p_{\text{ext}} e^{i\boldsymbol{k}\cdot\boldsymbol{x}}$

(c) $p(\boldsymbol{x}) = p_{\text{eff}} e^{i\boldsymbol{k}\cdot\boldsymbol{x}}$

Figure 4.1: Conceptual illustration of the source-driven homogenization procedure. (a) Externally controlled body forces and volume velocity sources impose an arbitrary $(\omega, \boldsymbol{k})$ pair in the background fluid. (b) The introduction of inhomogeneities result in a total field that is a combination of scattered and externally imposed fields. The scattered fields are not shown to minimize clutter, and the representative volume element analyzed in Chapter 4 is denoted by the red box. (c) The homogenized media can be described with dynamic effective parameters and same imposed $(\omega, \boldsymbol{k})$ dependence.

mentum (3.4) and mass (3.5) under an $e^{i\boldsymbol{k}\cdot\boldsymbol{x}} e^{-i\omega t}$ driven condition become

$$\begin{aligned} i\boldsymbol{k} p_{\text{ext}} &= i\omega\rho_0 \boldsymbol{u}_{\text{ext}} + \boldsymbol{f}_{\text{ext}}, \\ i\boldsymbol{k}\cdot\boldsymbol{u}_{\text{ext}} &= i\omega\beta_0 p_{\text{ext}} + q_{\text{ext}}, \end{aligned} \tag{4.1}$$

where p_{ext} and $\boldsymbol{u}_{\text{ext}}$ are the complex amplitudes of the acoustic pressure and particle velocity fields, respectively, that result from the externally controlled

dipole $\boldsymbol{f}_{\text{ext}}e^{i\boldsymbol{k}\cdot\boldsymbol{x}}$ and monopole $q_{\text{ext}}e^{i\boldsymbol{k}\cdot\boldsymbol{x}}$ source distributions. The space and time dependences $e^{i\boldsymbol{k}\cdot\boldsymbol{x}}e^{-i\omega t}$ of the fields have been suppressed in Equation (4.1).

Introducing a random distribution of small inhomogeneities into the fluid with the same externally controlled source distribution, as illustrated in Figure 4.1b, the conservation equations can be expressed as

$$\begin{aligned} \nabla p(\boldsymbol{x}) &= i\omega\rho_0\boldsymbol{u}(\boldsymbol{x}) + i\omega\boldsymbol{D}(\boldsymbol{x}) + \boldsymbol{f}_{\text{ext}}e^{i\boldsymbol{k}\cdot\boldsymbol{x}}, \\ \nabla\cdot\boldsymbol{u}(\boldsymbol{x}) &= i\omega\beta_0 p(\boldsymbol{x}) - i\omega M(\boldsymbol{x}) + q_{\text{ext}}e^{i\boldsymbol{k}\cdot\boldsymbol{x}}. \end{aligned} \tag{4.2}$$

These relationships determine the microscopic fields at every point in the medium in terms of the dipole polarization, $\boldsymbol{D}(\boldsymbol{x}) = [\rho(\boldsymbol{x}) - \rho_0]\,\boldsymbol{u}(\boldsymbol{x})$, and monopole polarization, $M(\boldsymbol{x}) = -[\beta(\boldsymbol{x}) - \beta_0]\,p(\boldsymbol{x})$. The polarizations account for the contrast in density and compressibility between the background medium and the inhomogeneities.

Using continuous source distributions to impose an arbitrary $(\omega, \boldsymbol{k})$ pair, one may assume that the effective field amplitudes for a representative volume element are uniquely determined [14–16] by

$$\begin{aligned} i\boldsymbol{k}p_{\text{eff}} &= i\omega\rho_0\boldsymbol{u}_{\text{eff}} + i\omega\boldsymbol{D}_{\text{eff}} + \boldsymbol{f}_{\text{ext}}, \\ i\boldsymbol{k}\cdot\boldsymbol{u}_{\text{eff}} &= i\omega\beta_0 p_{\text{eff}} - i\omega M_{\text{eff}} + q_{\text{ext}}, \end{aligned} \tag{4.3}$$

where $\boldsymbol{D}_{\text{eff}}$ and M_{eff} are the effective dipole and monopole polarizations, respectively. This is guaranteed for periodic arrays. An effective field distribution in the homogenized media is shown in Figure 4.1c, which has the same spatial dependence as the homogeneous background media, Figure 4.1a, however the field amplitudes are different, *i.e.*, $p_{\text{ext}} \neq p_{\text{eff}}$, due to the presence of microscale

inhomogeneities. By comparing Equation (4.3) and the conventional continuity expressions in Equations (3.4) and (3.5), the constitutive relations relating effective fields in the homogenized medium can be written as

$$\begin{aligned} \boldsymbol{\mu}_{\text{eff}} &= \rho_0 \boldsymbol{u}_{\text{eff}} + \boldsymbol{D}_{\text{eff}}, \\ \varepsilon_{\text{eff}} &= -\beta_0 p_{\text{eff}} + M_{\text{eff}}, \end{aligned} \tag{4.4}$$

where $\boldsymbol{\mu}_{\text{eff}}$ and ε_{eff} are the effective momentum density and volume strain field amplitudes, respectively. The challenge of determining the effective parameters of the homogenized medium, therefore, lies in relating the polarizations, $\boldsymbol{D}_{\text{eff}}$ and M_{eff}, to the properties of the inhomogeneities, their distribution in the background fluid, and the effective fields p_{eff} and $\boldsymbol{u}_{\text{eff}}$.

Procedures to reduce Equation (4.2) to a set of macroscopic dynamic equations for an effective medium as in Equation (4.3), have been discussed at length for periodic [15, 17, 19, 37, 38] and non-periodic [16] inhomogeneous media. All these procedures involve some form of field averaging over a representative volume element, illustrated by the red box in Figure 4.1b. Of particular interest, Alù [15] demonstrated in the analogous case in electromagnetism that a simple volume average removing the dominant Fourier components from Equation (4.2) is not sufficient to account for nonlocal effects, which are important in determining the effective dynamic properties of metamaterials, and developed a Taylor expansion procedure that would account for nonlocal effects. An important result of this procedure is that it demonstrates explicitly that $\boldsymbol{D}(\boldsymbol{x}) = 0$ does not imply $\boldsymbol{D}_{\text{eff}} = 0$, likewise $M(\boldsymbol{x}) = 0$ does not imply $M_{\text{eff}} = 0$. If the analogy holds for acoustic wave

phenomena, one would expect, for example, an uniform waveguide lined with array of shunt Helmholtz resonators will result in an effective compressibility *and* density different from the fluid in the waveguide, contrary to what is commonly presented in the literature. This is a result of nonlocal effects, which is demonstrated in the derivation and results that follow in this work. It is important to note that the Taylor series expansion method has recently been partially adopted for acoustic systems [39]; although, the expansion was not carried out sufficiently to account for nonlocal coupling and was only used to illustrate that one would expect bianisotropy due to even coupling to exist in acoustic media.

A relation between effective and externally imposed fields is found by subtracting Equation (4.1) from Equation (4.3) and by solving for the effective field amplitudes, which yields

$$\begin{aligned} \boldsymbol{u}_{\text{eff}} &= \boldsymbol{u}_{\text{ext}} + \underline{\boldsymbol{K}}_{\text{d}} \cdot \frac{\boldsymbol{D}_{\text{eff}}}{\rho_0} - \boldsymbol{K}_{\text{c}} \frac{1}{Z_0} \frac{M_{\text{eff}}}{\beta_0}, \\ p_{\text{eff}} &= p_{\text{ext}} + \boldsymbol{K}_{\text{c}} \cdot Z_0 \frac{\boldsymbol{D}_{\text{eff}}}{\rho_0} - K_{\text{m}} \frac{M_{\text{eff}}}{\beta_0}, \end{aligned} \tag{4.5}$$

where polarization weights, identified as $\underline{\boldsymbol{K}}_{\text{d}}$, K_{m}, and $\boldsymbol{K}_{\text{c}}$, are defined as

$$\begin{aligned} \underline{\boldsymbol{K}}_{\text{d}} &= \frac{(k_0^2 - \boldsymbol{k} \cdot \boldsymbol{k})\, \underline{\boldsymbol{I}} + \boldsymbol{k} \otimes \boldsymbol{k}}{\boldsymbol{k} \cdot \boldsymbol{k} - k_0^2}, \\ \boldsymbol{K}_{\text{c}} &= \frac{k_0 \boldsymbol{k}}{\boldsymbol{k} \cdot \boldsymbol{k} - k_0^2}, \\ K_{\text{m}} &= \frac{k_0^2}{\boldsymbol{k} \cdot \boldsymbol{k} - k_0^2}. \end{aligned} \tag{4.6}$$

Here, $\underline{\boldsymbol{I}}$ is the identity matrix of appropriate dimensions, and $k_0 = \omega\sqrt{\rho_0 \beta_0}$ and $Z_0 = \sqrt{\rho_0/\beta_0}$ are the characteristic wavenumber and characteristic impedance

of the background medium, respectively. Beginning with the polarization weights in Equation (4.5) and throughout the remainder of the present work, the subscript 'd' will be used to identify dipole quantities that relate dipole response contributions to particle velocity (dipole) fields, the subscript 'm' will be used to identify monopole quantities that relate monopole response contributions to pressure (monopole) fields, and the subscript 'c' will be used to identify coupling quantities that relate monopole response contributions to dipole fields and dipole response contributions to monopole fields.

In Equation (4.5), p_{eff} is function of dipole polarization through to the presence of $\boldsymbol{K}_{\text{c}}$, and $\boldsymbol{u}_{\text{eff}}$ is a function of monopole polarization through the presence of $\boldsymbol{K}_{\text{c}}$. For $\boldsymbol{k} \to 0$, the quasi-static limit, $\underline{\boldsymbol{K}}_{\text{d}} = -\underline{\boldsymbol{I}}$, $K_{\text{m}} = -1$, and $\boldsymbol{K}_{\text{c}} = 0$. It is only in this limit that the effective velocity field is a function of the dipole polarization alone and that the effective pressure field is a function of the monopole polarization alone. As pointed out by Alù [15] in electromagnetism, "an inherent form of [*Willis*] *coupling at the unit cell level* stems from weak spatial dispersion effects when [$\boldsymbol{k} \neq 0$], associated with finite phase velocity across each unit cell." As discussed in Section 2.2, odd coupling (nonlocal Willis coupling) in acoustics results from finite phase changes across the representative volume element. This effect is indicated by the presence of $\boldsymbol{K}_{\text{c}}$ in Equation (4.5), and $\boldsymbol{K}_{\text{c}}$ is indeed odd in $\boldsymbol{k}$.

The analysis above has shown that Willis coupling will exist in acoustics if the coupled polarization weight $\boldsymbol{K}_{\text{c}} \neq 0$, which is solely due to the non-zero phase across the unit cell. However, neither the composition nor the locations

of the inhomogeneities has been investigated. The response and interaction of the inhomogeneities will be considered in the sections that follow in order to determine the *effective* material parameters of the acoustic metamaterial.

4.2 Microscale effects: inhomogeneity response

In order to realize reciprocal metamaterials with the extreme properties discussed in Chapter 1, certain assumptions must hold true for the dynamic microstructure. Thus, inhomogeneities will be assumed (i) to satisfy reciprocity, (ii) to be acoustically small, *i.e.*, $k_0 l \ll 1$, where l is its representative length of the inhomogeneity, and (iii) to be well represented by point dipole, $\boldsymbol{d_n}$, and monopole, $m_{\boldsymbol{n}}$, moments, *i.e.*, quadrapole and higher order responses are negligible. The subscript $\boldsymbol{n}$ is a vector identifying a particular inhomogeneity. The dipole moment, $\boldsymbol{d_n}$, represents the dipole scattering strength of the $\boldsymbol{n}$th inhomogeneity, and the monopole moment, $m_{\boldsymbol{n}}$, represents its the monopole scattering strength.

First considering the inhomogeneity located at the origin, the local fields p_{loc} and $\boldsymbol{u}_{\text{loc}}$ are defined as the pressure and velocity fields that would exist at the origin in the absence of the inhomogeneity. The dipole and monopole moments of the inhomogeneity are related to the local fields via a response denoted simply as the "polarizabilities," which depend on the composition and geometry of the inhomogeneity. Polarizabilities have units of volume and may be determined from an analysis of scattered fields from a single inhomogeneity in isolation. The process to determine polarizabilities for 1D cases is provided

in Appendix B. The dipole and monopole moments of the inhomogeneity at the origin are given by

$$\begin{aligned} \frac{\boldsymbol{d_0}}{\rho_0} &= \underline{\boldsymbol{\alpha}}_{\mathrm{d}} \cdot \boldsymbol{u}_{\mathrm{loc}} - i\boldsymbol{\alpha}_{\mathrm{c}} \frac{1}{Z_0} p_{\mathrm{loc}}, \\ \frac{m_{\boldsymbol{0}}}{\beta_0} &= -i\boldsymbol{\alpha}_{\mathrm{c}} \cdot Z_0 \boldsymbol{u}_{\mathrm{loc}} - \alpha_{\mathrm{m}} p_{\mathrm{loc}}, \end{aligned} \tag{4.7}$$

where $\underline{\boldsymbol{\alpha}}_{\mathrm{d}}$ is the dipole polarizability that relates the local particle velocity to the dipole moment, α_{m} is the monopole polarizability that relates the local pressure to the monopole moment, and $\boldsymbol{\alpha}_{\mathrm{c}}$ is the coupled polarizability that relates the local particle velocity to the monopole moment and the local pressure to the dipole moment.

Equation (4.7) provides a more formal description of the coupled response of the inhomogeneity presented in Figure 2.2a of Section 4.5. The equivalent circuit in Figure 2.2b demonstrates that when $\boldsymbol{u}_{\mathrm{loc}} = 0$ but $p_{\mathrm{loc}} \neq 0$ the inhomogeneity only responds with monopolar motion if it is symmetric, *i.e.*, $\boldsymbol{d_0} = 0$ in this case, and responds with both monopolar and dipolar motion if it is asymmetric, *i.e.*, $\boldsymbol{d_0} \neq 0$ for an asymmetric inhomogeneity even though $\boldsymbol{u}_{\mathrm{loc}} = 0$. From the discussion of Figure 2.2, it is clear that the polarizabilities $\underline{\boldsymbol{\alpha}}_{\mathrm{d}}$ and α_{m} represent the pure dipole and monopole responses of the inhomogeneity, respectively, and that the coupled polarizability $\boldsymbol{\alpha}_{\mathrm{c}}$ is a response of the inhomogeneity that is only non-zero when the inhomogeneity has some form of asymmetry (parameter distribution or geometric). Therefore, $\boldsymbol{\alpha}_{\mathrm{c}}$ embodies the coupled scattering demonstrated in Figure 2.2 and will be shown to be directly related to even coupling in Section 4.5.

In order to solve for *effective* material parameters, Equation (4.7) must be inverted, such that the local fields are expressed in terms of the dipole and monopole moments as

$$\begin{aligned} \boldsymbol{u}_{\mathrm{loc}} &= \underline{\tilde{\boldsymbol{\alpha}}}_{\mathrm{d}} \cdot \frac{\boldsymbol{d_0}}{\rho_0} - i\tilde{\boldsymbol{\alpha}}_{\mathrm{c}} \frac{1}{Z_0} \frac{m_{\boldsymbol{0}}}{\beta_0}, \\ p_{\mathrm{loc}} &= -i\tilde{\boldsymbol{\alpha}}_{\mathrm{c}} \cdot Z_0 \frac{\boldsymbol{d_0}}{\rho_0} - \tilde{\alpha}_{\mathrm{m}} \frac{m_{\boldsymbol{0}}}{\beta_0}, \end{aligned} \tag{4.8}$$

where complementary polarizabilities, $\underline{\tilde{\boldsymbol{\alpha}}}_{\mathrm{d}}$, $\tilde{\alpha}_{\mathrm{m}}$, and $\tilde{\boldsymbol{\alpha}}_{\mathrm{c}}$, are defined as

$$\begin{aligned} \underline{\tilde{\boldsymbol{\alpha}}}_{\mathrm{d}} &= \underline{\boldsymbol{\alpha}}_{\mathrm{d}}^{-1} \left[\underline{\boldsymbol{I}} + \boldsymbol{\alpha}_{\mathrm{c}} \otimes \tilde{\boldsymbol{\alpha}}_{\mathrm{c}} \right], \\ \tilde{\alpha}_{\mathrm{m}} &= \alpha_{\mathrm{m}}^{-1} / \Delta_{\alpha}, \\ \tilde{\boldsymbol{\alpha}}_{\mathrm{c}} &= \boldsymbol{\alpha}_{\mathrm{c}} \cdot \left(\alpha_{\mathrm{m}} \underline{\boldsymbol{\alpha}}_{\mathrm{d}} \right)^{-1} / \Delta_{\alpha}, \end{aligned} \tag{4.9}$$

and $\Delta_{\alpha} = 1 - \boldsymbol{\alpha}_{\mathrm{c}} \cdot \left(\alpha_{\mathrm{m}} \underline{\boldsymbol{\alpha}}_{\mathrm{d}} \right)^{-1} \cdot \boldsymbol{\alpha}_{\mathrm{c}}$. Because $\tilde{\boldsymbol{\alpha}}_{\mathrm{c}}$ is proportional to $\boldsymbol{\alpha}_{\mathrm{c}}$, a symmetric inhomogeneity has complementary polarizabilities given by $\tilde{\boldsymbol{\alpha}}_{\mathrm{c}} = \boldsymbol{\alpha}_{\mathrm{c}} = 0$, $\underline{\tilde{\boldsymbol{\alpha}}}_{\mathrm{d}} = \underline{\boldsymbol{\alpha}}_{\mathrm{d}}^{-1}$, and $\tilde{\alpha}_{\mathrm{m}} = \alpha_{\mathrm{m}}^{-1}$, and only in the symmetric case, $\underline{\tilde{\boldsymbol{\alpha}}}_{\mathrm{d}}$ and $\tilde{\alpha}_{\mathrm{m}}$ represent pure dipole and monopole responses, respectively. For $\tilde{\boldsymbol{\alpha}}_{\mathrm{c}} \neq 0$, the local velocity and pressure fields are dependent on both monopole and dipole moments and monopole, dipole, and coupled polarizabilities due to the presence of Δ_{α} in Equation (4.9).

Like the polarizabilities, the components of the complementary polarizabilities, $\underline{\tilde{\boldsymbol{\alpha}}}_{\mathrm{d}}$, $\tilde{\alpha}_{\mathrm{m}}$, and $\tilde{\boldsymbol{\alpha}}_{\mathrm{c}}$, are functions of the geometry and the material parameters that make up the inhomogeneities. The complementary polarizabilities are therefore independent of the direction of the imposed wavevector, $\boldsymbol{k}$, and thus *even* in $\boldsymbol{k}$. As one may therefore expect, the sections that follow demonstrate that $\tilde{\boldsymbol{\alpha}}_{\mathrm{c}}$ is directly related to macroscopic even coupling as described in Sections 2.1 and 2.2.

4.3 Mesoscale effects: multiple scattering

Having defined the monopole and dipole moments of a single inhomogeneity in the previous section, their contributions to the local fields of all other inhomogeneities must be determined in order to accurately represent the response of the entire inhomogeneous medium. This is very difficult in general since the local fields are the result of summations of the scattered fields from all inhomogeneities and the imposed fields, p_{ext} and $\boldsymbol{u}_{\text{ext}}$. In order to make it possible to calculate the local fields, inhomogeneities are assumed to be acoustically small ($k_0 l \ll 1$) and spaced sufficiently far apart such that near field scattering effects between inhomogeneities are negligible. For the initial formulation, the locations of inhomogeneities are arbitrary, although asymmetric inhomogeneities are assumed to be identical in size, composition, and orientation with respect to the global coordinate system. This assumption (identical inhomogeneities) requires that every inhomogeneity be defined by the same polarizabilities. The derivation of the local fields as a function of the imposed and scattered fields up to Equation (4.12) is otherwise general and may be specialized to 1-, 2-, or 3D depending on the choice of the scalar Green's function $g(\boldsymbol{x}|\boldsymbol{x_n})$, which is defined in Appendix A. The results of this section will be specialized to periodic lattices in Section 4.4.

For acoustically small inhomogeneities in the presence of an incident acoustic field, the scattered fields at a point $\boldsymbol{x_m}$ due to an inhomogeneity located at $\boldsymbol{x_n}$ maybe expressed in terms of the dipole and monopole moments of the $\boldsymbol{n}$th inhomogeneity and modified Green's functions with the following

expressions,

$$\begin{aligned} \boldsymbol{u}_{\mathrm{s}}(\boldsymbol{x}_{\boldsymbol{m}}) &= \underline{\boldsymbol{G}}_{\mathrm{d}}^{\boldsymbol{mn}} \cdot \frac{\boldsymbol{d}_{\boldsymbol{n}}}{\rho_0} - \boldsymbol{G}_{\mathrm{c}}^{\boldsymbol{mn}} \frac{1}{Z_0} \frac{m_{\boldsymbol{n}}}{\beta_0}, \\ p_{\mathrm{s}}(\boldsymbol{x}_{\boldsymbol{m}}) &= \boldsymbol{G}_{\mathrm{c}}^{\boldsymbol{mn}} \cdot Z_0 \frac{\boldsymbol{d}_{\boldsymbol{n}}}{\rho_0} - G_{\mathrm{m}}^{\boldsymbol{mn}} \frac{m_{\boldsymbol{n}}}{\beta_0}. \end{aligned} \tag{4.10}$$

The dipole modified Green's tensor $\underline{\boldsymbol{G}}_{\mathrm{d}}^{\boldsymbol{mn}}$ relates the inhomogeneity's dipole moment to the scattered particle velocity; the monopole modified Green's scalar $G_{\mathrm{m}}^{\boldsymbol{mn}}$ relates the inhomogeneity's monopole moment to the scattered pressure; and the coupled modified Green's vector $\boldsymbol{G}_{\mathrm{c}}^{\boldsymbol{mn}}$ relates the inhomogeneity's dipole moment to the scattered pressure and monopole moment to the scattered particle velocity.

The modified Green's functions are directly related to the scalar Green's function $g(\boldsymbol{x}|\boldsymbol{x}_{\boldsymbol{n}})$ for the reciprocal background fluid by

$$\begin{aligned} \underline{\boldsymbol{G}}_{\mathrm{d}}^{\boldsymbol{mn}} &= -\nabla\nabla g(\boldsymbol{x}|\boldsymbol{x}_{\boldsymbol{n}})|_{\boldsymbol{x}=\boldsymbol{x}_{\boldsymbol{m}}} = \underline{\boldsymbol{G}}_{\mathrm{d}}^{\boldsymbol{nm}} = (\underline{\boldsymbol{G}}_{\mathrm{d}}^{\boldsymbol{mn}})^{\mathrm{T}}, \\ \boldsymbol{G}_{\mathrm{c}}^{\boldsymbol{mn}} &= -ik_0 \nabla g(\boldsymbol{x}|\boldsymbol{x}_{\boldsymbol{n}})|_{\boldsymbol{x}=\boldsymbol{x}_{\boldsymbol{m}}} = -\boldsymbol{G}_{\mathrm{c}}^{\boldsymbol{nm}}, \\ G_{\mathrm{m}}^{\boldsymbol{mn}} &= k_0^2 g(\boldsymbol{x}_{\boldsymbol{m}}|\boldsymbol{x}_{\boldsymbol{n}}) = G_{\mathrm{m}}^{\boldsymbol{nm}}. \end{aligned} \tag{4.11}$$

The exchange of locations $\boldsymbol{x}_{\boldsymbol{n}} \leftrightarrow \boldsymbol{x}_{\boldsymbol{m}}$ represents scattering in the oppposite direction, and Equation (4.11) provides the corresponding changes. $\underline{\boldsymbol{G}}_{\mathrm{d}}^{\boldsymbol{mn}}$ and $G_{\mathrm{m}}^{\boldsymbol{mn}}$ are unchanged; however, $\boldsymbol{G}_{\mathrm{c}}^{\boldsymbol{mn}}$ undergoes a sign change due to the gradient operation. The sign change for a corresponding change in scattering direction indicates that this component of mesoscale interaction will be odd in wavevector. It will be shown in the following sections that $\boldsymbol{G}_{\mathrm{c}}^{\boldsymbol{mn}}$ contributes to macroscopic odd coupling.

The local fields may now be determined by the summation of the externally imposed fields and the fields scattered from all other inhomogeneities. It is most straightforward to consider an inhomogeneity located at the origin, $\boldsymbol{n} = \boldsymbol{0}$, where the local particle velocity and pressure, $\boldsymbol{u}_{\mathrm{loc}}$ and p_{loc}, may be expressed as

$$\begin{aligned} \boldsymbol{u}_{\mathrm{loc}} &= \boldsymbol{u}_{\mathrm{ext}} + \sum_{\boldsymbol{n}\neq\boldsymbol{0}} \left(\underline{\boldsymbol{G}}_{\mathrm{d}}^{\boldsymbol{0n}} \cdot \frac{\boldsymbol{d}_{\boldsymbol{n}}}{\rho_0} - \boldsymbol{G}_{\mathrm{c}}^{\boldsymbol{0n}} \frac{1}{Z_0} \frac{m_{\boldsymbol{n}}}{\beta_0} \right), \\ p_{\mathrm{loc}} &= p_{\mathrm{ext}} + \sum_{\boldsymbol{n}\neq\boldsymbol{0}} \left(\boldsymbol{G}_{\mathrm{c}}^{\boldsymbol{0n}} \cdot Z_0 \frac{\boldsymbol{d}_{\boldsymbol{n}}}{\rho_0} - G_{\mathrm{m}}^{\boldsymbol{0n}} \frac{m_{\boldsymbol{n}}}{\beta_0} \right). \end{aligned} \tag{4.12}$$

In order to quantify the scattering interaction between unit cells, one must determine the relation between moments of a pair of inhomogeneities, *i.e.*, the relations between the moments of the $\boldsymbol{i}$th and $\boldsymbol{j}$th inhomogeneities: $\boldsymbol{d}_{\boldsymbol{i}}$ and $\boldsymbol{d}_{\boldsymbol{j}}$, $\boldsymbol{d}_{\boldsymbol{i}}$ and $m_{\boldsymbol{j}}$, and $m_{\boldsymbol{i}}$ and $m_{\boldsymbol{j}}$. For an arbitrary array, this requires knowledge of the local fields at every inhomogeneity location, which is not possible in general. However, as demonstrated in the next section, the case of periodic arrays results in converging lattice sums, making it possible to quantify unit cell interaction.

4.4 Periodic array

The existence of an infinite periodic lattice of inhomogeneities significantly reduces the problem of quantifying the interaction between unit cells, and it suffices to proceed with the analysis on a single unit cell, which for simplicity will be centered on the origin. For the case of periodic arrays, the dipole and monopole moments of the $\boldsymbol{n}$th inhomogeneity are directly related

to the moments of the inhomogeneity at the origin through application of the Floquet condition: $\boldsymbol{d_n} = \boldsymbol{d_0} e^{i\boldsymbol{k}\cdot\boldsymbol{x_n}}$ and $m_{\boldsymbol{n}} = m_{\boldsymbol{0}} e^{i\boldsymbol{k}\cdot\boldsymbol{x_n}}$. Equations (4.12) are then given by

$$\begin{aligned} \boldsymbol{u}_{\mathrm{loc}} &= \boldsymbol{u}_{\mathrm{ext}} + \underline{\boldsymbol{C}}_{\mathrm{d}} \cdot \frac{\boldsymbol{d_0}}{\rho_0} - \boldsymbol{C}_{\mathrm{c}} \frac{1}{Z_0} \frac{m_{\boldsymbol{0}}}{\beta_0}, \\ p_{\mathrm{loc}} &= p_{\mathrm{ext}} + \boldsymbol{C}_{\mathrm{c}} \cdot Z_0 \frac{\boldsymbol{d_0}}{\rho_0} - C_{\mathrm{m}} \frac{m_{\boldsymbol{0}}}{\beta_0}, \end{aligned} \tag{4.13}$$

where the interaction coefficients, $\underline{\boldsymbol{C}}_{\mathrm{d}}$, C_{m}, and $\boldsymbol{C}_{\mathrm{c}}$, are defined by

$$\begin{aligned} \underline{\boldsymbol{C}}_{\mathrm{d}} &= \sum_{\boldsymbol{n}\neq 0} e^{i\boldsymbol{k}\cdot\boldsymbol{x_n}} \underline{\boldsymbol{G}}_{\mathrm{d}}^{\boldsymbol{0n}}, \\ \boldsymbol{C}_{\mathrm{c}} &= \sum_{\boldsymbol{n}\neq 0} e^{i\boldsymbol{k}\cdot\boldsymbol{x_n}} \boldsymbol{G}_{\mathrm{c}}^{\boldsymbol{0n}}, \\ C_{\mathrm{m}} &= \sum_{\boldsymbol{n}\neq 0} e^{i\boldsymbol{k}\cdot\boldsymbol{x_n}} G_{\mathrm{m}}^{\boldsymbol{0n}}. \end{aligned} \tag{4.14}$$

Each interaction coefficient in Equation (4.13) quantifies a different contribution to the local fields at the origin from the scattered fields from the infinite periodic array of inhomogeneities. The dipole interaction tensor of coefficients $\underline{\boldsymbol{C}}_{\mathrm{d}}$ quantifies the contributions to the local velocity at the origin related to the dipole moments $\boldsymbol{d_n}$ resulting from the local fields at locations $\boldsymbol{x_n}$ of all other inhomogeneities. Similarly, the monopole interaction coefficient C_{m} quantifies the contributions to the local pressure at the origin related to the monopole moments $m_{\boldsymbol{n}}$ resulting from the local fields at locations $\boldsymbol{x_n}$ of all other inhomogeneities, and the coupled interaction vector of coefficients $\boldsymbol{C}_{\mathrm{c}}$ quantifies the contributions to the local velocity at the origin related to the monopole moments $m_{\boldsymbol{n}}$ and contributions to the local pressure at the origin related to the dipole moments $\boldsymbol{d_n}$ resulting from the local fields at locations

$\boldsymbol{x_n}$ of all other inhomogeneities. It is important to note that these interaction coefficients are purely a function of the modified Green's functions, the periodic spatial distribution of the inhomogeneities, and the imposed wavevector. One can therefore determine these coefficients for any given lattice arrangement for which convergent lattice sum exists.

The externally imposed field amplitudes may now be expressed in terms of the complementary polarizabilities, interaction coefficients, and dipole and monopole moments by eliminating the local fields in (4.8) and (4.13) to yield

$$\begin{aligned} \boldsymbol{u}_{\text{ext}} &= (\underline{\tilde{\boldsymbol{\alpha}}}_{\text{d}} - \underline{\boldsymbol{C}}_{\text{d}}) \cdot \frac{\boldsymbol{d_0}}{\rho_0} - (i\tilde{\boldsymbol{\alpha}}_{\text{c}} - \boldsymbol{C}_{\text{c}}) \frac{1}{Z_0} \frac{m_{\boldsymbol{0}}}{\beta_0}, \\ p_{\text{ext}} &= (-i\tilde{\boldsymbol{\alpha}}_{\text{c}} - \boldsymbol{C}_{\text{c}}) \cdot Z_0 \frac{\boldsymbol{d_0}}{\rho_0} - (\tilde{\alpha}_{\text{m}} - C_{\text{m}}) \frac{m_{\boldsymbol{0}}}{\beta_0}. \end{aligned} \tag{4.15}$$

In the absence of the imposed fields, *i.e.*, $p_{\text{ext}} = 0$ and $\boldsymbol{u}_{\text{ext}} = 0$, Equation (4.15) can be rearranged into the following transcendental equation

$$(\tilde{\alpha}_{\text{m}} - C_{\text{m}}) (\underline{\tilde{\boldsymbol{\alpha}}}_{\text{d}} - \underline{\boldsymbol{C}}_{\text{d}}) \cdot \frac{\boldsymbol{d_0}}{\rho_0} - (i\tilde{\boldsymbol{\alpha}}_{\text{c}} - \boldsymbol{C}_{\text{c}}) \left[(-i\tilde{\boldsymbol{\alpha}}_{\text{c}} - \boldsymbol{C}_{\text{c}}) \cdot \frac{\boldsymbol{d_0}}{\rho_0} \right] = 0. \tag{4.16}$$

The solutions to (4.16) provide the eigenmodal pairs $(\omega, \boldsymbol{k})$ for any periodic array described by complementary polarizabilities and interaction coefficients. Though this expression is compact, it is important to re-iterate that it includes both microscale and mesoscale effects to determine macroscopic eigenmodal pairs. In other words, both the local response of the inhomogeneity and the nonlocal multiple scattering lattice contributions are included in this formulation. Only a few assumptions have been made to achieve the compact representation in Equation (4.16): (i) the background medium satisfies reciprocity,

and the inhomogeneities (*ii*) satisify reciprocity, are (*iii*) acoustically small, (*iv*) identically oriented, and (*v*) arranged periodically. Complementary polarizabilities and interaction coefficients are not trivial to find, but the derivation up to this point is exceptionally general.

Though the interaction coefficients contain infinite summations, they all have analytic representations for 1D periodic systems. To the author's knowledge, rapidly convergent series have been found for C_{m} and $\underline{\boldsymbol{C}}_{\mathrm{d}}$ for 2D and 3D cubic arrays [78], but are yet to be determined for $\boldsymbol{C}_{\mathrm{c}}$ or more general periodic lattices. For simplicity, the results presented here will be restricted to the 1D case, leaving more general cases for future work. It is important to emphasize, however, that the model derived here is completely general for 1-, 2-, and 3D periodic lattices, and therefore, the observations and the physical phenomena they illustrate apply to all cases where inhomogeneities are acoustically small and periodically distributed in a background medium.

4.5 Effective material parameters

As discussed in Section 4.1 and exemplified by the constitutive relations in Equation (4.4), the effective polarizations $\boldsymbol{D}_{\mathrm{eff}}$ and M_{eff} demonstrate how the effective media differs from the background fluid, where $\boldsymbol{D}_{\mathrm{eff}}$ is the additional momentum density and M_{eff} is the additional volume strain of the unit cell. The total response of the inhomogeneity quantifies this additional momentum density and volume strain. It was assumed in Section 4.2 that this total response could be represented by monopole and dipole motion, Equation

(4.7), which were quantified in terms of the composition and geometry of the inhomogeneity via polarizabilities as well as the total local field due to externally imposed fields and scattered fields via interaction coefficients. Generally, $\boldsymbol{D}_{\text{eff}}$ is the density of dipole moments in the unit cell, implying $\boldsymbol{D}_{\text{eff}} = \boldsymbol{d_0}/V$; M_{eff} is the density of monopole moments, or $M_{\text{eff}} = m_{\boldsymbol{0}}/V$; and V is the volume of the unit cell.

Combining Equations (4.5) and (4.15) and eliminating the imposed fields, the effective fields in terms of the polarizations are given by

$$\begin{aligned} \boldsymbol{u}_{\text{eff}} &= \underline{\tilde{\boldsymbol{\Lambda}}}_{\text{d}} \cdot \frac{\boldsymbol{D}_{\text{eff}}}{\rho_0} - \left(\tilde{\boldsymbol{\Lambda}}_{\text{c}}^{\text{o}} + i\tilde{\boldsymbol{\Lambda}}_{\text{c}}^{\text{e}}\right) \frac{1}{Z_0} \frac{M_{\text{eff}}}{\beta_0}, \\ p_{\text{eff}} &= \left(\tilde{\boldsymbol{\Lambda}}_{\text{c}}^{\text{o}} - i\tilde{\boldsymbol{\Lambda}}_{\text{c}}^{\text{e}}\right) \cdot Z_0 \frac{\boldsymbol{D}_{\text{eff}}}{\rho_0} - \tilde{\Lambda}_{\text{m}} \frac{M_{\text{eff}}}{\beta_0}, \end{aligned} \tag{4.17}$$

where

$$\begin{aligned} \underline{\tilde{\boldsymbol{\Lambda}}}_{\text{d}} &= V\underline{\tilde{\boldsymbol{\alpha}}}_{\text{d}} - V\underline{\boldsymbol{C}}_{\text{d}} + \underline{\boldsymbol{K}}_{\text{d}}, \\ \tilde{\Lambda}_{\text{m}} &= V\tilde{\alpha}_{\text{m}} - VC_{\text{m}} + K_{\text{m}}, \\ \tilde{\boldsymbol{\Lambda}}_{\text{c}}^{\text{o}} &= -V\boldsymbol{C}_{\text{c}} + \boldsymbol{K}_{\text{c}}, \\ \tilde{\boldsymbol{\Lambda}}_{\text{c}}^{\text{e}} &= V\tilde{\boldsymbol{\alpha}}_{\text{c}}. \end{aligned} \tag{4.18}$$

The tensor $\underline{\tilde{\boldsymbol{\Lambda}}}_{\text{d}}$ only consists of terms relating dipole fields, and the scalar $\tilde{\Lambda}_{\text{m}}$ only consists of terms relating monopole fields. All of the components of $\underline{\tilde{\boldsymbol{\Lambda}}}_{\text{d}}$ and $\tilde{\Lambda}_{\text{m}}$ are even with respect to propagation direction. Noting the signs in front of the two vectors containing coupling terms, $\tilde{\boldsymbol{\Lambda}}_{\text{c}}^{\text{o}}$ and $\tilde{\boldsymbol{\Lambda}}_{\text{c}}^{\text{e}}$, in Equation (4.17), one might naturally separate the terms comprising these vectors. However from the detailed analysis of the preceding sections, the components of

$\tilde{\boldsymbol{\Lambda}}_{\mathrm{c}}^{\mathrm{o}}$ are both mesoscale effects and odd with respect to a reversal of propagation, whereas $\tilde{\boldsymbol{\Lambda}}_{\mathrm{c}}^{\mathrm{e}}$ is due asymmetry at the microscale and even with respect to propagation, as presented in Equation (4.18).

To determine effective parameters, Equation (4.17) must be inverted, expressing effective polarizations in terms of effective fields as

$$\begin{aligned}\frac{\boldsymbol{D}_{\mathrm{eff}}}{\rho_0} &= \underline{\boldsymbol{\Lambda}}_{\mathrm{d}} \cdot \boldsymbol{u}_{\mathrm{eff}} - \left(\boldsymbol{\Lambda}_{\mathrm{c}}^{\mathrm{o}} + i\boldsymbol{\Lambda}_{\mathrm{c}}^{\mathrm{e}}\right) \frac{1}{Z_0} p_{\mathrm{eff}}, \\ \frac{M_{\mathrm{eff}}}{\beta_0} &= \left(\boldsymbol{\Lambda}_{\mathrm{c}}^{\mathrm{o}} - i\boldsymbol{\Lambda}_{\mathrm{c}}^{\mathrm{e}}\right) \cdot Z_0 \boldsymbol{u}_{\mathrm{eff}} - \Lambda_{\mathrm{m}} p_{\mathrm{eff}},\end{aligned} \tag{4.19}$$

where

$$\begin{aligned}\underline{\boldsymbol{\Lambda}}_{\mathrm{d}} &= \underline{\tilde{\boldsymbol{\Lambda}}}_{\mathrm{d}}^{-1} \left[\underline{\boldsymbol{I}} + \left(\tilde{\boldsymbol{\Lambda}}_{\mathrm{c}}^{\mathrm{o}} + i\tilde{\boldsymbol{\Lambda}}_{\mathrm{c}}^{\mathrm{e}}\right) \otimes \left(\boldsymbol{\Lambda}_{\mathrm{c}}^{\mathrm{o}} - i\boldsymbol{\Lambda}_{\mathrm{c}}^{\mathrm{e}}\right)\right], \\ \boldsymbol{\Lambda}_{\mathrm{c}}^{\mathrm{e}} &= \tilde{\boldsymbol{\Lambda}}_{\mathrm{c}}^{\mathrm{e}} \cdot \left(\tilde{\Lambda}_{\mathrm{m}} \underline{\tilde{\boldsymbol{\Lambda}}}_{\mathrm{d}}\right)^{-1} / \Delta_{\tilde{\Lambda}}, \\ \boldsymbol{\Lambda}_{\mathrm{c}}^{\mathrm{o}} &= \tilde{\boldsymbol{\Lambda}}_{\mathrm{c}}^{\mathrm{o}} \cdot \left(\tilde{\Lambda}_{\mathrm{m}} \underline{\tilde{\boldsymbol{\Lambda}}}_{\mathrm{d}}\right)^{-1} / \Delta_{\tilde{\Lambda}}, \\ \Lambda_{\mathrm{m}} &= \tilde{\Lambda}_{\mathrm{m}}^{-1} / \Delta_{\tilde{\Lambda}},\end{aligned} \tag{4.20}$$

and $\Delta_{\tilde{\Lambda}} = 1 - (\tilde{\boldsymbol{\Lambda}}_{\mathrm{c}}^{\mathrm{o}} - i\tilde{\boldsymbol{\Lambda}}_{\mathrm{c}}^{\mathrm{e}}) \cdot (\tilde{\Lambda}_{\mathrm{m}} \underline{\tilde{\boldsymbol{\Lambda}}}_{\mathrm{d}})^{-1} \cdot (\tilde{\boldsymbol{\Lambda}}_{\mathrm{c}}^{\mathrm{o}} + i\tilde{\boldsymbol{\Lambda}}_{\mathrm{c}}^{\mathrm{e}})$. Equations (4.7) and (4.19) may be thought of as macro-micro pairs where the macroscopic expression, Equation (4.19), contains information about the micro- and mesoscale physics.

Substituting the polarizations provided by Equation (4.19) into the constitutive relations given by Equation (4.4), yields

$$\begin{aligned}\boldsymbol{\mu}_{\mathrm{eff}} &= \underline{\boldsymbol{\rho}}_{\mathrm{eff}} \cdot \boldsymbol{u}_{\mathrm{eff}} - \left(\boldsymbol{\chi}_{\mathrm{eff}}^{\mathrm{o}} + i\boldsymbol{\chi}_{\mathrm{eff}}^{\mathrm{e}}\right) p_{\mathrm{eff}}, \\ \varepsilon_{\mathrm{eff}} &= \left(\boldsymbol{\chi}_{\mathrm{eff}}^{\mathrm{o}} - i\boldsymbol{\chi}_{\mathrm{eff}}^{\mathrm{e}}\right) \cdot \boldsymbol{u}_{\mathrm{eff}} - \beta_{\mathrm{eff}} p_{\mathrm{eff}},\end{aligned} \tag{4.21}$$

where

$$\begin{aligned}
\frac{\underline{\boldsymbol{\rho}}_{\text{eff}}}{\rho_0} &= \underline{\boldsymbol{I}} + \underline{\boldsymbol{\Lambda}}_{\text{d}}, \\
\frac{\beta_{\text{eff}}}{\beta_0} &= 1 + \Lambda_{\text{m}}, \\
c_0 \boldsymbol{\chi}^{\text{o}}_{\text{eff}} &= \boldsymbol{\Lambda}^{\text{o}}_{\text{c}}, \\
c_0 \boldsymbol{\chi}^{\text{e}}_{\text{eff}} &= \boldsymbol{\Lambda}^{\text{e}}_{\text{c}},
\end{aligned} \tag{4.22}$$

which have the same form the bianisotropic relations in electromagnetism Equation (2.1) and the Willis relations in elastodynamics Equation (2.3). The effective density tensor $\underline{\boldsymbol{\rho}}_{\text{eff}}$ relates the effective velocity to the effective momentum; the effective compressibility scalar β_{eff} relates the effective pressure to the effective volume strain; and the odd and even effective coupling vectors $\boldsymbol{\chi}^{\text{o}}_{\text{eff}}$ and $\boldsymbol{\chi}^{\text{e}}_{\text{eff}}$ relate the effective pressure to the effective momentum and the effective velocity to the effective volume strain.

Due to the inversion required to derive Equation (4.19), all the effective parameters are, to some order, a function of every microscale response and mesoscale interaction. Although to first order, $\Delta_{\tilde{\Lambda}} \approx 1$, which leads to $\underline{\boldsymbol{\Lambda}}_{\text{d}} \approx \underline{\tilde{\boldsymbol{\Lambda}}}_{\text{d}}^{-1}$, $\Lambda_{\text{m}} \approx \tilde{\Lambda}_{\text{m}}^{-1}$, $\boldsymbol{\Lambda}^{\text{o}}_{\text{c}} \approx \tilde{\boldsymbol{\Lambda}}^{\text{o}}_{\text{c}} \cdot (\tilde{\Lambda}_{\text{m}} \underline{\tilde{\boldsymbol{\Lambda}}}_{\text{d}})^{-1}$, and $\boldsymbol{\Lambda}^{\text{e}}_{\text{c}} \approx \tilde{\boldsymbol{\Lambda}}^{\text{e}}_{\text{c}} \cdot (\tilde{\Lambda}_{\text{m}} \underline{\tilde{\boldsymbol{\Lambda}}}_{\text{d}})^{-1}$. Therefore, in this limit, the effective density is only related to dipole effects; effective compressibility only related to monopole effects; odd coupling is related to mesoscale effects and monopole and dipole effects; and even coupling is related to microscale effects and monopole and dipole effects. As discussed in Section 4.2, a symmetric inhomogeneity results in $\tilde{\boldsymbol{\alpha}}_{\text{c}} = 0$, and therefore, from Equations (4.18), (4.20), and (4.22), $\boldsymbol{\chi}^{\text{e}}_{\text{eff}} = 0$. However, there will still be odd coupling, $\boldsymbol{\chi}^{\text{o}}_{\text{eff}} \neq 0$, due to unit cell interaction and finite phase speed

across the unit cell, which in general may not be neglected. If it is neglected, the calculated effective parameters may lose physical meaning [15, 23], which is demonstrated in the following chapter.

The homogenization procedure presented in this chapter is quite general, with only a few simplifying assumptions. The polarizabilities of a few canonical geometries are available analytically, and their value may be calculated with full-wave simulations for complex inclusions. Also, the interaction coefficients are available in closed-form for only a few periodic lattice geometries. In Chapter 5, exact solutions for polarizabilities and interaction coefficients are obtained for 1D, and examples are considered that demonstrate the utility of the approach and the need to include effective material properties with coupled constitutive relationships.

Chapter 5

Source-Free 1D Examples

Evaluating the polarizabilities introduced in Equation (4.7) and the interaction coefficients introduced in Equation (4.14) presents a challenging numerical problem and is a primary drawback of multiple scattering models. However, for 1D periodic media, these features have exact closed-form expressions, which reveal the odd and even nature of the coupling parameters in bianisotropic fluids. Additionally, 1D acoustics experiments may be easily developed, simulated, and solved analytically using scalar transmission line techniques, such as transmission and scattering matrices [79]. An example, source-free, 1D periodic medium with period L is depicted in Figure 5.1, where longitudinal plane wave propagation is assumed along the x-axis, which is indicated by the unit vector $\hat{x}$. The background media has properties ρ_0 and β_0 and representative cross-sectional area A, and the inhomogeneities are composed of N-layers with the jth layer characterized by $\rho_j(\omega)$, $\beta_j(\omega)$, length l_j, and cross-section A_j, where $\sum_{j=1}^{N} l_j = l$ is the total length of the inhomogeneity. The cross-sectional area A cancels out in the parameters derivation, and the cross-section of the inhomogeneity layers are allowed differ from the background region because changes of cross-section are commonly used in acoustic waveguide experiments, *e.g.*, Reference [80].

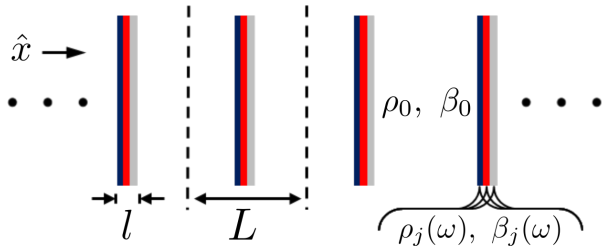

Figure 5.1: Schematic of source-free 1D periodic medium with plane wave propagation along the x-axis, period L, background parameters β_0 and ρ_0, total inhomogeneity size l, and inhomogeneity properties $\rho_j(\omega)$ and $\beta_j(\omega)$.

Results and analyses in this chapter are presented and discussed in terms of the normalized quantities k_0L and $\boldsymbol{k}L$, and it is important to keep in mind what these quantities represent. The quantity $k_0L = \omega L\sqrt{\rho_0\beta_0}$ is the operating frequency normalized by the background fluid properties and unit cell dimension L, whereas $\boldsymbol{k}L$ is the wavevector of the imposed field normalized by L or, in the absence of a source distribution, a macroscopic wavevector satisfying the transcendental equation for the array, Equation (4.16). This chapter proceeds as follows. Section 5.1 introduces the 1D *effective* parameters based on the derivation of the previous chapter. In the absence of sources, the macroscopic parameters are non-unique [14–16], and therefore, Section 5.2 serves to introduce two alternative macroscopic descriptions referred to as *equivalent* and *Bloch*. In Section 5.3, parameters are numerically calculated for three example periodic media, and the *effective*, *equivalent*, and *Bloch* macroscopic descriptions are presented and discussed in light of the restrictions on macroscopic material parameters, which are summarized in Section 3.5. The results of the numerical examples are discussed in Section 5.4.

5.1 1D effective material parameters

The following sections provide insight into *effective* material parameters derived in Chapter 4. The even and odd natures of the two coupling parameters stemming from the polarizabilities and interaction coefficients are verified; the specific acoustic impedance and effective wavenumber are defined in terms of effective parameters; and leading order terms are derived.

5.1.1 Polarizabilities and interaction coefficients

The polarizabilities for a 1D, N-layer inhomogeneity may be exactly determined from the scattering matrix of a single inhomogeneity in the background medium. The derivation is outlined in Appendix B, and the polarizabilities defined in Equation (4.7) are given by

$$\begin{aligned} \alpha_{\mathrm{d}} &= \frac{S_{12} - e^{ik_0 l} - \left(S_{22} + S_{11}\right)/2}{ik_0/A} e^{-ik_0 l}, \\ \boldsymbol{\alpha}_{\mathrm{c}} &= \hat{x} \frac{\left(S_{22} - S_{11}\right)/2}{k_0/A} e^{-ik_0 l} = \hat{x}\alpha_{\mathrm{c}}, \\ \alpha_{\mathrm{m}} &= \frac{S_{12} - e^{ik_0 l} + \left(S_{22} + S_{11}\right)/2}{ik_0/A} e^{-ik_0 l}, \end{aligned} \tag{5.1}$$

where $\hat{x}$ is the unit vector for the propagation axis. There are two important takeaways from Equation (5.1). First, because l is finite, the presence of $e^{-ik_0 l}$ demonstrates that polarizabilities map the exact scattered fields from a finite inhomogeneity to its center thereby representing the inhomogeneity as an infinitesimal point scatterer. Representing the finite inhomogeneity as a point introduces a violation of causality for the polarizabilities, which can be corrected [81]; however, this effect is negligible for small inhomogeneities

compared to the violations of causality introduced by ignoring even and odd coupling [15]. The analysis of the causality of the polarizabilities is beyond the scope of this work. Secondly, the expression for $\boldsymbol{\alpha}_\mathrm{c}$ explicitly shows that the vector nature of this term is defined by the coordinate system, and that it is even in wavevector. This confirms the statements made in the previous chapter. Using Equation (4.9), the 1D complementary polarizabilities are given by

$$\begin{aligned}
\tilde{\alpha}_\mathrm{d} &= \alpha_\mathrm{d}^{-1} / \left(1 - \alpha_\mathrm{d}^{-1}\alpha_\mathrm{m}^{-1}\alpha_\mathrm{c}^2\right), \\
\tilde{\boldsymbol{\alpha}}_\mathrm{c} &= \hat{x}\alpha_\mathrm{c}\alpha_\mathrm{d}^{-1}\alpha_\mathrm{m}^{-1} / \left(1 - \alpha_\mathrm{d}^{-1}\alpha_\mathrm{m}^{-1}\alpha_\mathrm{c}^2\right) = \hat{x}\tilde{\alpha}_\mathrm{c}, \\
\tilde{\alpha}_\mathrm{m} &= \alpha_\mathrm{m}^{-1} / \left(1 - \alpha_\mathrm{d}^{-1}\alpha_\mathrm{m}^{-1}\alpha_\mathrm{c}^2\right).
\end{aligned} \tag{5.2}$$

The interaction coefficients defined in Equation (4.14) also may be solved exactly in 1D. If inhomogeneities are located at positions $\boldsymbol{x_n} = \hat{x}nL$, where n is an integer $(-\infty, \infty)$, the interaction coefficients defined in Equation (4.14) and normalized by V reduce to

$$\begin{aligned}
VC_\mathrm{d} = VC_\mathrm{m} &= \frac{k_0 L}{2}\frac{\sin\left(k_0 L\right)}{\cos\left(k_0 L\right) - \cos\left(\hat{x}\cdot\boldsymbol{k}L\right)} - i\frac{k_0 L}{2}, \\
V\boldsymbol{C}_\mathrm{c} &= \hat{x}\frac{k_0 L}{2}\frac{\sin\left(\hat{x}\cdot\boldsymbol{k}L\right)}{\cos\left(k_0 L\right) - \cos\left(\hat{x}\cdot\boldsymbol{k}L\right)},
\end{aligned} \tag{5.3}$$

as shown in Appendix C. The dependencies on $\boldsymbol{k}L$ in Equation (5.3) clearly demonstrate that monopole and dipole interaction coefficients are independent of propagation direction, whereas the coupled interaction coefficient is indeed odd in $\boldsymbol{k}$. Additionally, the expressions for C_d and C_m are always complex, but $\boldsymbol{C}_\mathrm{c}$ is purely real for real k_0 and $\boldsymbol{k}$. The eigenvalues of the array are found

by substituting Equation (5.3) into Equation (4.16), which yields

$$\cos(kL) = a\cos(k_0 L) - \frac{k_0 L}{2} b \sin(k_0 L), \tag{5.4}$$

where

$$\begin{aligned} a &= \frac{\left(V\tilde{\alpha}_{\mathrm{m}} + i\frac{k_0 L}{2}\right)\left(V\tilde{\alpha}_{\mathrm{d}} + i\frac{k_0 L}{2}\right) - \left(V\tilde{\alpha}_{\mathrm{c}}\right)^2 - \left(\frac{k_0 L}{2}\right)^2}{\left(V\tilde{\alpha}_{\mathrm{m}} + i\frac{k_0 L}{2}\right)\left(V\tilde{\alpha}_{\mathrm{d}} + i\frac{k_0 L}{2}\right) - \left(V\tilde{\alpha}_{\mathrm{c}}\right)^2 + \left(\frac{k_0 L}{2}\right)^2}, \\ b &= \frac{\left(V\tilde{\alpha}_{\mathrm{m}} + i\frac{k_0 L}{2}\right) + \left(V\tilde{\alpha}_{\mathrm{d}} + i\frac{k_0 L}{2}\right)}{\left(V\tilde{\alpha}_{\mathrm{m}} + i\frac{k_0 L}{2}\right)\left(V\tilde{\alpha}_{\mathrm{d}} + i\frac{k_0 L}{2}\right) - \left(V\tilde{\alpha}_{\mathrm{c}}\right)^2 + \left(\frac{k_0 L}{2}\right)^2}. \end{aligned} \tag{5.5}$$

Passivity requires that the imaginary parts of the inhomogeneities satisfy $\mathrm{Im}(V\tilde{\alpha}_{\mathrm{d}}) \leq -k_0 L/2$ and $\mathrm{Im}(V\tilde{\alpha}_{\mathrm{m}}) \leq -k_0 L/2A$, where equality occurs when the inhomogeneity is lossless; also, $\mathrm{Im}(V\tilde{\alpha}_{\mathrm{c}}) = 0$ when the inhomogeneity is lossless (see Appendix D). The the factor $-k_0 L/2$ in $\mathrm{Im}(V\tilde{\alpha}_{\mathrm{d}})$ and $\mathrm{Im}(V\tilde{\alpha}_{\mathrm{m}})$ represents the re-radiation from the inhomogeneity, and for lossless inhomogeneities in a periodic array, this term cancels the identical term in the interaction coefficients, Equation (5.3), when they are subtracted in the homogenization procedure, Equation (4.15), due to coherent scattering. This cancellation is also observed in the eigenvalue expressions in Equation (5.5). In fact, the imaginary parts of the complementary polarizabilities and interaction coefficients cancel for any lossless periodic media in 1-, 2-, or 3D. For non-periodic inhomogeneous media, the imaginary parts will not cancel and scattering losses will be present in effective parameters even if all constituents are lossless [75].

5.1.2 Wavenumber and impedance

For periodic media in the absence of sources, the $(\omega, \boldsymbol{k})$ solutions are the eigenvalues of Equation (4.16), and for 1D, $\boldsymbol{k} = \hat{x}k$, where k is the Bloch wavenumber of the array and is given by Equation (5.4). Suppressing the unit vector $\hat{x}$, the constitutive relations for 1D become

$$\begin{aligned} \mu_{\text{eff}} &= \rho_{\text{eff}} u_{\text{eff}} - \left(\chi^{\text{o}}_{\text{eff}} + i\chi^{\text{e}}_{\text{eff}}\right) p_{\text{eff}}, \\ \varepsilon_{\text{eff}} &= \left(\chi^{\text{o}}_{\text{eff}} - i\chi^{\text{e}}_{\text{eff}}\right) u_{\text{eff}} - \beta_{\text{eff}} p_{\text{eff}}. \end{aligned} \tag{5.6}$$

The relation between the effective parameters and the wavenumber may be determined directly from the conservation equations, Equations (3.4) and (3.5), in the absence of sources, which leads to

$$\left(k/\omega + \chi^{\text{o}}_{\text{eff}}\right)^2 = \rho_{\text{eff}}\beta_{\text{eff}} - \left(\chi^{\text{e}}_{\text{eff}}\right)^2, \tag{5.7}$$

and therefore,

$$k^{\pm}/\omega = \pm\sqrt{\rho_{\text{eff}}\beta_{\text{eff}} - \left(\chi^{\text{e}}_{\text{eff}}\right)^2} - \chi^{\text{o}\pm}_{\text{eff}}, \tag{5.8}$$

where $\pm$ correspond to waves traveling in $\pm\hat{x}$-directions. Notice that for the representation of constitutive relations in Equation (5.6), the wavenumber is a function of all effective parameters (this is not the case for other forms of the constitutive relations, *e.g.*, References [17], [24], and [47]), and odd coupling is direction-dependent.

The specific acoustic impedance, derived from the conservation of momentum, may be expressed as

$$\begin{aligned} Z^{\pm} = \frac{p_{\text{eff}}}{u_{\text{eff}}} &= \frac{\rho_{\text{eff}}}{\left(k/\omega + \chi^{\text{o}}_{\text{eff}}\right) + i\chi^{\text{e}}_{\text{eff}}}, \\ &= \pm\sqrt{\frac{\rho_{\text{eff}}}{\beta_{\text{eff}}} - \left(\frac{\chi^{\text{e}}_{\text{eff}}}{\beta_{\text{eff}}}\right)^2} - i\frac{\chi^{\text{e}}_{\text{eff}}}{\beta_{\text{eff}}}, \end{aligned} \tag{5.9}$$

which for a passive medium must satisfy $\mathrm{Re}(Z^+) \geq 0$ and $\mathrm{Re}(Z^-) \leq 0$. Surprisingly, Equation (5.9) indicates that if even coupling exists the impedance will be complex, even if the medium is lossless, and that the phase angle changes with direction. All of which is not intuitive. However, periodic media with asymmetric unit cells have long been shown to have complex *Bloch* impedances [82], which will be discussed in more detail in Section 5.2, and it has previously been demonstrated that the specific acoustic impedance must always be complex in Willis materials with even coupling [39, 47, 83]. The complex nature of the impedance make Willis materials with even coupling ideal for impedance matching applications, as demonstrated by Koo *et al.* [39].

Equations (5.8) and (5.9) demonstrate that one cannot determine density and compressibility from only impedance and wavenumber when there exists non-zero coupling, *i.e.*, $\rho_{\mathrm{eff}} \neq Z^{\pm}k^{\pm}/\omega$ and $\beta_{\mathrm{eff}} \neq k^{\pm}/(\omega Z^{\pm})$, which is counter to general assumptions in reflection/transmission extraction methods for acoustical parameters [65].

5.1.3 Leading order terms

At this point it is informative to provide some insight into the relationships between the *effective* material parameters and the volume averaged parameters, which are usually used to estimate the overall response of an inhomogeneous medium. Specifically, understanding how the coupling terms relate to the volume averaged density and compressibility demonstrates that these terms may not be negligible even in the long wavelength limit.

Leading order terms for the quasi-static limit, $k_0 L \to 0$ and $kL \to 0$, are determined for the effective material parameters from Taylor expansions of polarizabilities and interaction coefficients. In this limit, the jth material of a multi-layer inhomogeneity may be described by its lumped acoustic mass $M_j^{\mathrm{A}} = \rho_j l_j / A_j$ and acoustic compliance $C_j^{\mathrm{A}} = \beta_j l_j A_j$. For this case, leading order terms of the effective parameters in terms of acoustic mass and compliance are

$$\begin{aligned}
\rho_{\mathrm{eff}}/\rho_0 &\to 1 - l/L + \sum_{j=1}^{N} \frac{M_j^{\mathrm{A}}}{M_0^{\mathrm{A}}} = \frac{\langle \rho \rangle}{\rho_0}, \\
\beta_{\mathrm{eff}}/\beta_0 &\to 1 - l/L + \sum_{j=1}^{N} \frac{C_j^{\mathrm{A}}}{C_0^{\mathrm{A}}} = \frac{\langle \beta \rangle}{\beta_0}, \\
c_0 \chi_{\mathrm{eff}}^{\mathrm{e}} &\to \frac{k_0 L}{2} \sum_{i=1}^{N-1} \sum_{j=i+1}^{N} \frac{M_i^{\mathrm{A}} C_j^{\mathrm{A}} - M_j^{\mathrm{A}} C_i^{\mathrm{A}}}{M_0^{\mathrm{A}} C_0^{\mathrm{A}}}, \\
c_0 \chi_{\mathrm{eff}}^{\mathrm{o}} &\to \frac{(k_0 L)\,(kL)}{12} \left(\frac{\langle \rho \rangle}{\rho_0} - 1 \right) \left(\frac{\langle \beta \rangle}{\beta_0} - 1 \right),
\end{aligned} \tag{5.10}$$

where $M_0^{\mathrm{A}} = \rho_0 L / A$ and $C_0^{\mathrm{A}} = \beta_0 L A$ are the acoustic mass and compliance of the unit cell in the absence of the inhomogeneity, *i.e.*, a volume $V = LA$ of the background media. As might be expected, the effective density and compressibility are constants in the quasi-static limit and are provided by the volume averaged values. However, the coupling parameters are not constants. Even coupling is proportional to frequency, $k_0 L$, and odd coupling is proportional to frequency multiplied by the macroscopic wavenumber, $(k_0 L)(kL)$. For $(k_0 L)(kL) < 0.1$, the effects of odd coupling are likely to be negligible. These limiting results verify that odd and even coupling are indeed higher order effects.

Additionally, the frequency dependence of even coupling suggests that time derivative, $-i\omega$, has been absorbed into $\chi^{\mathrm{e}}_{\mathrm{eff}}$ due to the way the constitutive relations are expressed in Equation (5.6). Nassar *et al.* [38] and Muhlestein *et al.* [24] noticed similar results and suggested that modified constitutive relations would be more meaningful for time-domain studies. Additionally, the frequency and wavenumber dependence of odd coupling suggests that both time and spatial derivatives have been absorbed into $\chi^{\mathrm{o}}_{\mathrm{eff}}$. As pointed out by Muhlestein *et al.* [24], an analysis of causality suggests that parameters be constant in the quasistatic limit. Therefore, a more meaningful form of the constitutive relations for time domain study may be

$$\begin{aligned} \boldsymbol{\mu}_{\mathrm{eff}} &= \underline{\boldsymbol{\rho}}_{\mathrm{eff}} \cdot \boldsymbol{u}_{\mathrm{eff}} - \left(\underline{\boldsymbol{\phi}}_{\mathrm{eff}} \cdot \nabla \dot{p}_{\mathrm{eff}} - \boldsymbol{\theta}_{\mathrm{eff}} \dot{p}_{\mathrm{eff}} \right), \\ \varepsilon_{\mathrm{eff}} &= \left(\underline{\boldsymbol{\phi}}_{\mathrm{eff}} : \nabla \dot{\boldsymbol{u}}_{\mathrm{eff}} + \boldsymbol{\theta}_{\mathrm{eff}} \cdot \dot{\boldsymbol{u}}_{\mathrm{eff}} \right) - \beta_{\mathrm{eff}} p_{\mathrm{eff}}, \end{aligned} \tag{5.11}$$

which are related to the previously defined coefficients by $\boldsymbol{\chi}^{\mathrm{e}}_{\mathrm{eff}} = \omega \boldsymbol{\theta}_{\mathrm{eff}}$ and $\boldsymbol{\chi}^{\mathrm{o}}_{\mathrm{eff}} = \omega \underline{\boldsymbol{\phi}}_{\mathrm{eff}} \cdot \boldsymbol{k}$, and $\boldsymbol{\theta}_{\mathrm{eff}}$ and $\underline{\boldsymbol{\phi}}_{\mathrm{eff}}$ are both even functions in wavenumber and constant in the quasistatic limit.

In general, the form of the constitutive relations used are out of convenience. For this work, constitutive relations were expressed in terms of p and $\boldsymbol{u}$, because these variables are most commonly used in acoustics, and this form is the most analogous to the common E-H convention in electromagnetism [69].

5.2 Alternative macroscopic descriptions

In the absence of sources, the constitutive relations are non-unique, allowing for alternative macroscopic descriptions. The following subsections

provide a description that relates effective fields but neglects coupling, referred to as *equivalent* parameters, and a description related to the microscopic fields, referred to as *Bloch* parameters.

5.2.1 Equivalent parameters

The constitutive relations for *equivalent* parameters have the same form as a traditional homogeneous fluid, *i.e.*,

$$\begin{aligned} \mu_{\text{eff}} &= \rho_{\text{eq}} u_{\text{eff}}, \\ \varepsilon_{\text{eff}} &= -\beta_{\text{eq}} p_{\text{eff}}, \end{aligned} \tag{5.12}$$

and correspondingly,

$$k^{\pm}/\omega = \pm\sqrt{\rho_{\text{eq}}^{\pm}\beta_{\text{eq}}^{\pm}}, \tag{5.13}$$

$$Z^{\pm} = \pm\sqrt{\rho_{\text{eq}}^{\pm}/\beta_{\text{eq}}^{\pm}}. \tag{5.14}$$

As indicated, the *equivalent* parameters are directionally dependent. This can be seen more clearly by considering the relation between *effective* and *equivalent* parameters, which by using Equation (5.6) and (5.12) and the conservation equations leads to

$$\begin{aligned} \rho_{\text{eq}}^{\pm} &= \rho_{\text{eff}} \left(1 + \frac{\chi_{\text{eff}}^{\text{o}\pm} + i\chi_{\text{eff}}^{\text{e}}}{k^{\pm}/\omega}\right)^{-1} = Z^{\pm}k^{\pm}/\omega, \\ \beta_{\text{eq}}^{\pm} &= \beta_{\text{eff}} \left(1 + \frac{\chi_{\text{eff}}^{\text{o}\pm} - i\chi_{\text{eff}}^{\text{e}}}{k^{\pm}/\omega}\right)^{-1} = k^{\pm}/\omega Z^{\pm}. \end{aligned} \tag{5.15}$$

Equation (5.15) provides several insights. First, *equivalent* parameters are determined directly from wavenumber and impedance. Second, in the absence of even coupling, *equivalent* density and compressibility are not directionally dependent, but still differ from the effective properties due to finite

odd coupling. However, for non-zero even coupling, *equivalent* density and compressibility will be directionally dependent and complex even for lossless media, in which case the imaginary part of one will be greater than zero (normally indicative of loss) and the imaginary part of the other will be less than zero (normally indicative of gain) depending on the sign of $\chi^{\mathrm{e}}_{\mathrm{eff}}$ in Equation (5.15).

These observations suggest that, while *equivalent* parameters provide knowledge of wave propagation by their relation to impedance and wavenumber, the *equivalent* parameters themselves lack physical meaning by violating passivity and possibly causality (Section 3.5).

5.2.2 Bloch parameters

Transmission line analogs have been widely used in the development and understanding of 1D periodic acoustic metamaterials [83–86], and because they maintain the microscopic fields at the boundary of a defined unit cell [83], transmission line models lend themselves well to measurement via the reflection/transmission method popularized by Fokin *et al.* [65] that was recently extended to account for asymmetry [39, 47]. However, homogenization schemes, such as the one developed in Chapter 4, determine effective fields that do not necessarily equal microscopic fields at any point. Therefore, the parameters determined by employing transmission line techniques and reflection/transmission measurements are not *effective* or *equivalent* parameters, as defined in this work, but are *Bloch* parameters that relate the boundary

fields of an unit cell defined by the transmission matrix [83] or measurement sample [47, 65]. As *Bloch* parameters do not relate effective fields but instead microscopic fields at the unit cell boundary defined by the study, they cannot account for nonlocal effects, and therefore, will not satisfy the restrictions due to causality.

It was demonstrated in the classic work by Brillouin [82] that the *Bloch* impedance changes with position, and if the position results in an asymmetric unit cell, the *Bloch* impedance will be complex. In 1D periodic acoustic media, the microscopic field patterns due to time-harmonic waves are *Bloch* waves [82]. This was demonstrated in 1D periodic acoustic media by Bradley both theoretically [87] and experimentally [80]. Therefore, one may express the *Bloch* impedance, which is the ratio of the microscopic pressure and particle velocity at a position x, as [22, 82, 83]

$$Z^{\pm}_{\mathrm{B}(x)} = \frac{p(x)}{u(x)} = \pm\sqrt{\frac{\rho_{\mathrm{B}(x)}}{\beta_{\mathrm{B}(x)}} - \left(\frac{\chi^{\mathrm{e}}_{\mathrm{B}(x)}}{\beta_{\mathrm{B}(x)}}\right)^2} - i\frac{\chi^{\mathrm{e}}_{\mathrm{B}(x)}}{\beta_{\mathrm{B}(x)}}. \tag{5.16}$$

In periodic media, the *Bloch* wavenumber is the solution to the transcendental equation, Equation (4.16) or (5.4), and is related to *Bloch* parameters via

$$k^{\pm}/\omega = \pm\sqrt{\rho_{\mathrm{B}(x)}\beta_{\mathrm{B}(x)} - \left(\chi^{\mathrm{e}}_{\mathrm{B}(x)}\right)^2}. \tag{5.17}$$

In summary, unlike *effective* and *equivalent* properties, *Bloch* properties (i) only exist for periodic media and (ii) relate the microscopic fields at a point rather than effective fields. While it is convenient for measurements to relate parameters to boundary fields, such an approach does not necessarily lead

to physically meaningful parameters that satisfy passivity and causality, as is demonstrated in the following section.

5.3 Numerical examples

This section presents three 1D periodic media examples without embedded sources. Therefore, macroscopic parameters are non-unique, and wavenumbers are the eigenvalues of the lattice determined by Equation (5.4) or from transmission matrices [79]. Under these conditions, the *effective* material parameters (Section 5.1) may be directly compared to the two alternative macroscopic descriptions (Section 5.2) referred to as *equivalent* material parameters, which relate effective fields but neglect coupling, and *Bloch* material parameters, which relate microscopic fields the boundaries of a specific unit cell and cannot account for nonlocal effects. The solutions are presented for longitudinal wave propagation normal to the layers, in the $\hat{x}$-direction, as indicated in Figure 5.1. For this case, purely transverse or longitudinal elastic wave behavior is entirely consistent with the acoustic wave conservation equations used in this work.

Figures 5.2–5.5, 5.7, and 5.8 present normalized macroscopic material parameters plotted versus normalized frequency $k_0 L$ obtained using the *effective* (solid lines), *equivalent* (dash-dot lines), and *Bloch* (dashed lines) models for forward propagation in the $+\hat{x}$-direction. In all of these figures, the background shading highlights frequency ranges of interest: (i) white for $|\mathrm{Re}(kL)| < 1$ corresponding to wavenumbers for which dynamic homogeniza-

tion is generally accepted [22]; (*ii*) light gray for $1 \leq \mathrm{Re}(kL) < \pi$ corresponding to wavenumbers that some suggest [38, 88] are reasonable to apply dynamic homogenization; and (*iii*) dark gray corresponding to stop bands. Unless otherwise noted, material properties were obtained from Appendix A of Reference [67], and material compressibility was calculated using $\beta = 1/(\rho c^2)$. The results are discussed in light of physical restrictions summarized in Section 3.5.

5.3.1 Lead inhomogeneities in aluminum

The first example is a two-phase composite consisting of lead inhomogeneities ($\rho_{\mathrm{Pb}} = 11300$ kg/m^3, $c_{\mathrm{Pb}} = 2050$ m/s) embedded in aluminum ($\rho_{\mathrm{Al}} = 2700$ kg/m^3, $c_{\mathrm{Al}} = 6300$ m/s) with filling fraction $l/L = 0.1$. Additionally, both lead and aluminum are assumed lossless; therefore in propagating bands, all macroscopic material parameters should be purely real.

Figure 5.2 presents the normalized wavenumber (top), density (middle), and compressibility (bottom). Two unit cell configurations were used to calculate *Bloch* parameters, which are depicted in the insert in the top panel of Figure 5.2. Configuration (1) corresponds to the inhomogeneity being centered in the unit cell, and configuration (2) corresponds to an asymmetric cell configuration with the inhomogeneity on the right. For the product $(k_0 L)(kL) < 0.1$, which approximately corresponds to $k_0 L < 0.3$ in this example, the macroscopic density and compressibility for the four models converged to volume-averaged quantities but diverged for $k_0 L > 0.3$ due to odd coupling from nonlocal effects. Additionally, negative slopes were observed in the den-

sity computed using the *Bloch* (2) model and in the compressibility computed using the the *equivalent* and *Bloch* (1) models, which indicates that only the *effective* model satisfies causality for this medium, as defined by Equation (3.24), even in the quasi-static limit.

Normalized even and odd coupling are presented in the top and bottom panels of Figure 5.3, respectively. Because the presence of asymmetry in a two-phase medium is a feature of a particularly defined unit cell, $\chi^{\mathrm{e}} = 0$ for the *effective* and *Bloch* (1) models but is finite for the *Bloch* (2) model. Only the *effective* model can account for nonlocal effects, and even though $c_0\chi^{\mathrm{o}}_{\mathrm{eff}}/(k_0LkL)$ is small, it is non-zero and grows rapidly for $k_0L > 2$.

5.3.2 Steel and rubber inhomogeneities in water

The second example is a three-phase composite consisting of steel ($\rho_{\mathrm{st}} = 7700$ kg/m^3, $c_{\mathrm{st}} = 6100$ m/s) and rubber ($\rho_{\mathrm{ru}} = 1100$ kg/m^3, $c_{\mathrm{ru}} = 2400$ m/s) inhomogeneities embedded in water ($\rho_{\mathrm{w}} = 998$ kg/m^3, $c_{\mathrm{w}} = 1481$ m/s), where all materials are assumed to be lossless. The inhomogeneities consisted of equal parts steel and rubber, *i.e.*, $l_{\mathrm{st}} = l_{\mathrm{ru}}$, and the total size of the inhomogeneities, $l = l_{\mathrm{st}} + l_{\mathrm{ru}}$, was varied from $l/L = 0.01$ to $l/L = 0.5$. A 1D three-phase composite always has an asymmetric unit cell regardless of how the unit cell is drawn; therefore, even coupling should be observed.

The normalized wavenumber (top), density (middle), and compressibility (bottom) for $l/L = 0.2$ are presented in Figure 5.4, and the *Bloch* parameters were calculated with inhomogeneity centered in the unit cell as

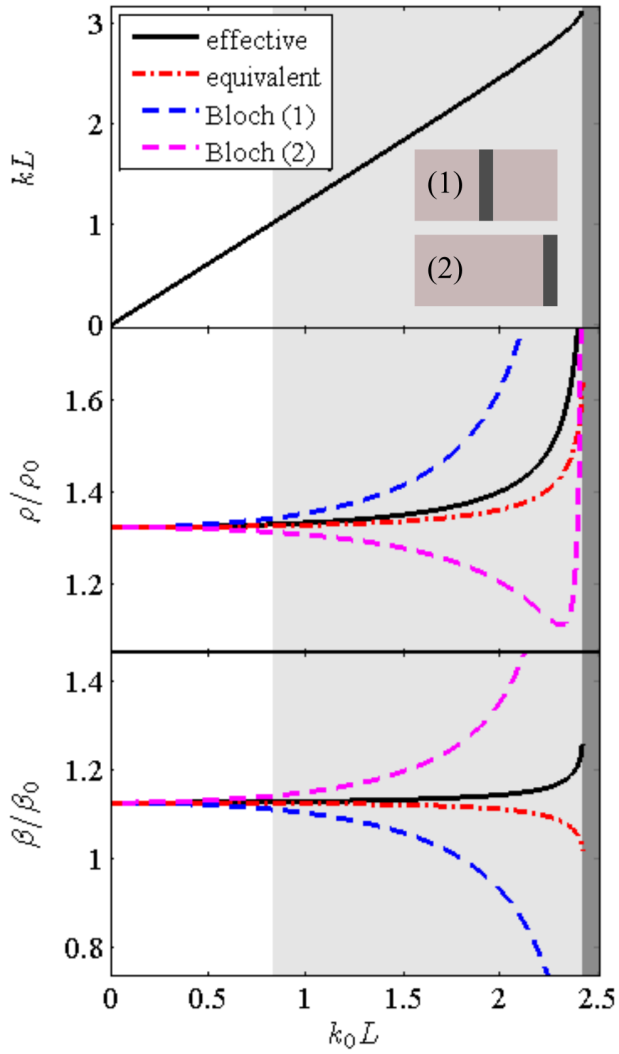

Figure 5.2: Normalized macroscopic wavenumber (top), mass density (middle), and compressibility (bottom) plotted versus normalized frequency for an 1D periodic medium with lead inhomogeneities in an aluminum background, and $l/L = 0.1$. Two different unit cells were used to determine *Bloch* parameters: Bloch (1) corresponds to the inhomogeneity being centered in the unit cell, and Bloch (2) corresponds to the inhomogeneity at the unit cell boundary, as depicted in the insert of the top panel.

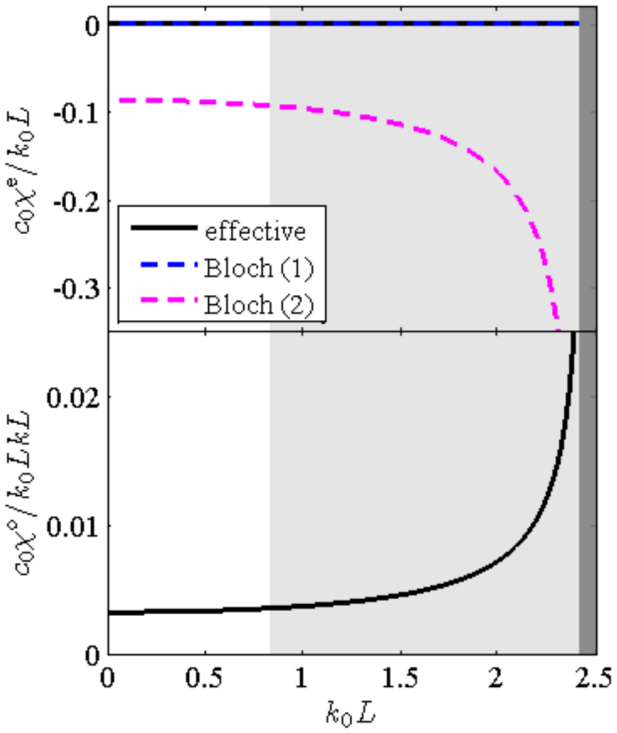

Figure 5.3: Normalized macroscopic coupling, even (top) and odd (bottom), plotted versus normalized frequency for an 1D periodic medium with lead inhomogeneities in an aluminum background, and $l/L = 0.1$.

depicted in the insert in the top panel. Similar to the first example, the product $(k_0 L)(kL) < 0.1$ approximately corresponds to $k_0 L < 0.3$, and again, the models converged on the same values for the macroscopic density and compressibility below this frequency and diverged for $k_0 L > 0.3$ due to odd coupling from nonlocal effects. The only apparent causality violation, denoted by a negative slope, occurred in the compressibility calculated using the *Bloch* model.

Because the *equivalent* model does not account for even coupling, it

appears through complex parameters, which is counter to the fact that the composite is lossless. The insert between the middle and bottom panels of Figure 5.4 demonstrates that the imaginary parts of *equivalent* density and compressibility are non-zero. Additionally, $\mathrm{Im}(\beta_{\mathrm{eq}}) < 0$ which violates passivity, as shown in Equation (3.24), but the combination of *equivalent* density and compressibility result in passive k and Z. Again, only the *effective* density and compressibility satisfy causality and passivity for this composite.

Figure 5.5 presents normalized even (top) and odd (bottom) coupling plotted versus normalized frequency. The *Bloch* even coupling determined from the unit cell centered on the inhomogeneity matches the *effective* even coupling in the quasi-static limit but diverges for $k_0 L > 0.3$ similar to density and compressibility. Again, $c_0 \chi^{\mathrm{o}}_{\mathrm{eff}}/(k_0 L k L)$ is small, but non-zero, and grows rapidly for $k_0 L > 1.5$.

Figure 5.6 presents normalized *effective* even (top) and odd (bottom) coupling plotted versus volume fraction, l/L, for several wavenumbers. Both coupling parameters increase in magnitude as $(l/L)^2$, and normalized forms are relatively constant for $kL \leq 1$, suggesting that the limits for $\chi^{\mathrm{e}}_{\mathrm{eff}}$ and $\chi^{\mathrm{o}}_{\mathrm{eff}}$ in Equation (5.10) may be valid for $kL \leq 1$. To be consistent, however, one must also consider second order effects, $(k_0 L)^2$ and $(kL)^2$, in ρ_{eff} and β_{eff}, which are not included in the expressions in Equation (5.10).

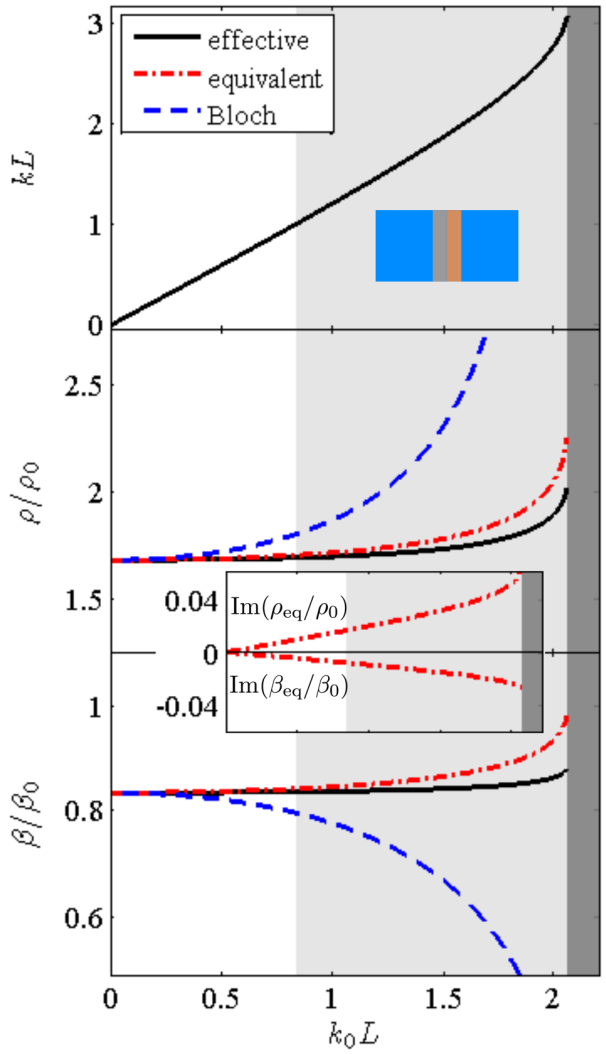

Figure 5.4: Normalized macroscopic wavenumber (top), mass density (middle), and compressibility (bottom) plotted versus normalized frequency for an 1D periodic medium with inhomogeneities consisting of equal parts steel and rubber in an aqueous background, and $l/L = 0.2$. The Bloch parameters correspond to the inhomogeneity being centered in the unit cell, indicated by the top panel insert. The insert between the middle and bottom panels presents the normalized imaginary parts of the *equivalent* density and compressibility.

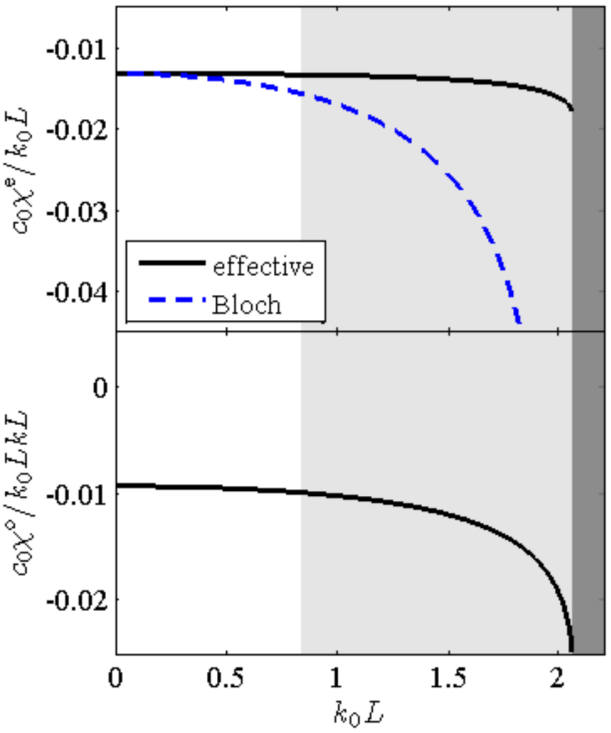

Figure 5.5: Normalized macroscopic even coupling (top) and odd coupling (bottom) plotted versus normalized frequency for an 1D periodic medium with inhomogeneities consisting of equal parts steel and rubber in an aqueous background, and $l/L = 0.2$.

5.3.3 Double negative inhomogeneities in air

Lastly, a four-phase composite exhibiting a double negative frequency band is considered and modeled such that it could be implemented with a rigid-walled waveguide with Helmholtz resonators in shunt and flexible plates in series, similar to the study by Seo *et al.* [85]. The inhomogeneities consist of three layers: (*i*) a region with dynamic compressibility, which models a Helmholtz resonator in shunt, (*ii*) a segment of air-filled waveguide, and (*iii*)

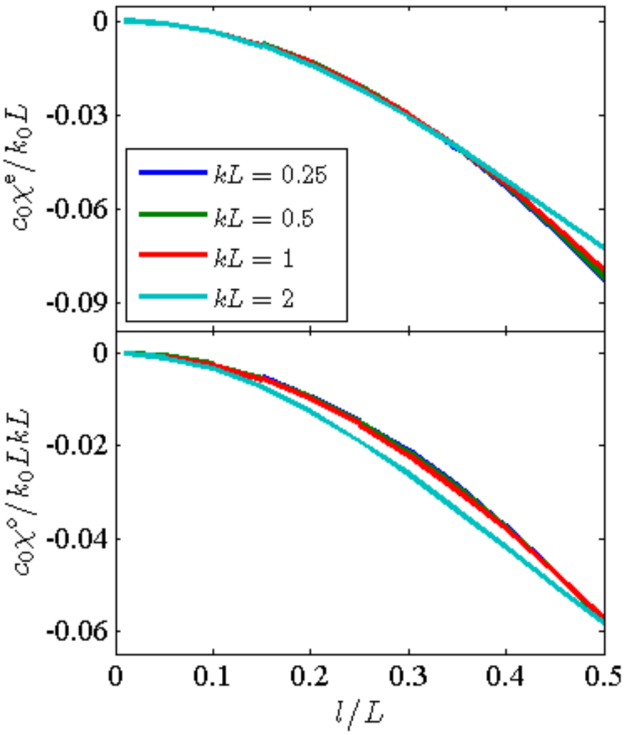

Figure 5.6: Normalized *effective* even coupling (top) and odd coupling (bottom) plotted versus inhomogeneity size for an 1D periodic medium with inhomogeneities consisting of equal parts steel and rubber in an aqueous background. Different colored lines correspond to coupling calculated for different wavenumbers: $kL = 0.25, 0.5, 1, 2$.

a region with dynamic density, which models a flexible plate in series with the waveguide.

A Helmholtz resonator in shunt can be modeled as a region with dynamic compressibility [89] with properties defined by $\rho_{\mathrm{H}} = \rho_{\mathrm{air}}$, $l_{\mathrm{H}}/L = 0.075$, and $\beta_{\mathrm{H}} = \beta_0 v_{\mathrm{H}}/[1 - i\omega_{\mathrm{H}}/(\omega Q_{\mathrm{H}}) - \omega^2/\omega_{\mathrm{H}}^2]$, where $v_{\mathrm{H}} = 10$, $\omega_{\mathrm{H}} L/c_0 = 0.25$, and $Q_{\mathrm{H}} = 20$. The waveguide segment was modeled as air-filled ($\rho_{\mathrm{air}} = 1.21$ kg/m^3,

$c_{\text{air}} = 343$ m/s) with length $l_{\text{air}}/L = 0.173$. The dynamic density region models a Kapton® plate [84] with $1/\beta_{\text{pl}} = E/[3(1-\nu)] = 1.3929$ GPa, $l_{\text{pl}}/L = 0.002$, and $\rho_{\text{pl}} = \rho_{\text{K}}[1 + i\omega_{\text{pl}}/(\omega Q_{\text{pl}}) - \omega_{\text{pl}}^2/\omega^2]$, where $\rho_{\text{K}} = 1420$ kg/m^3, $\omega_{\text{pl}}L/c_0 = 0.5$ and $Q_{\text{pl}} = 80$. The total relative size of the inhomogeneity was $l/L = 0.25$, where $l = l_{\text{H}} + l_{\text{air}} + l_{\text{pl}}$.

The normalized wavenumber (top), density (middle), and compressibility (bottom) are presented in Figure 5.7, and the *Bloch* parameters were calculated with the inhomogeneity centered in the unit cell as depicted in the insert in the top panel. Two passbands existed for this example: a double negative passband for $0.258 < k_0L < 0.334$, and a double positive passband for $k_0L > 0.419$. The inequality $(k_0L)|\text{Re}(kL)| < 0.1$ was satisfied in passband portions of the frequency range $0.3 < k_0L < 0.45$. Again it is near these bounds that the *Bloch* model begins to diverge from the *effective* model for both density and compressibility. Additionally, as observed in the middle panel of Figure 5.7, the *equivalent* density differed from the *Bloch* and *effective* densities in the double negative band even for small wavenumbers. This was not the case in the double positive passband, $k_0L > 0.419$, and might suggest that in highly dynamic passbands, which inevitably include double negative passbands, even and odd coupling are not negligible.

That even and odd coupling are not negligible is confirmed in Figure 5.8. In the double negative band, both coupling terms significantly exceed values observed in the previous two examples. Again, the *Bloch* even coupling determined from the unit cell centered on the inhomogeneity matches the

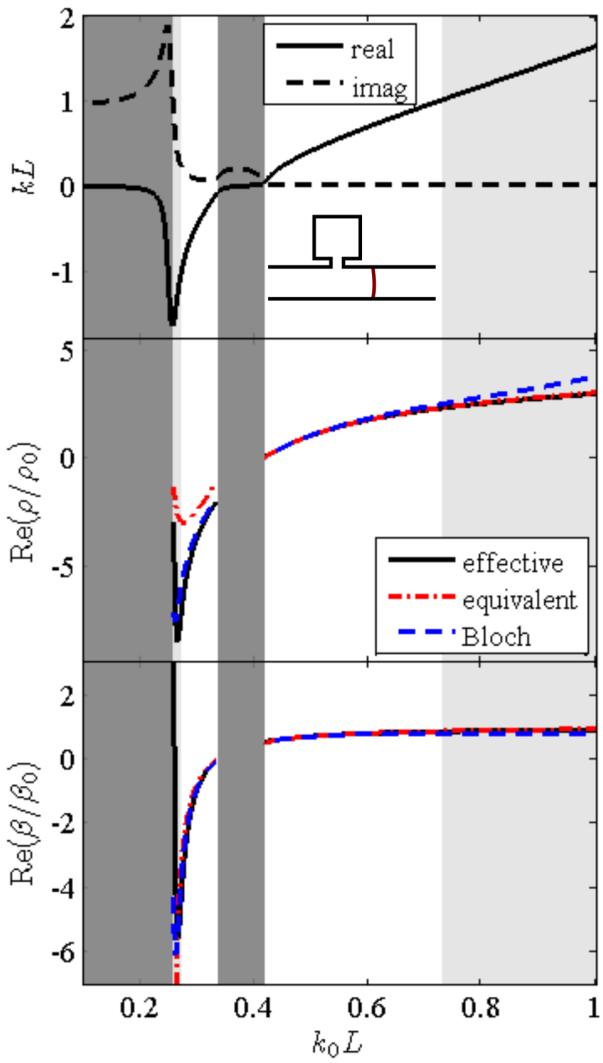

Figure 5.7: Normalized macroscopic wavenumber (top), mass density (middle), and compressibility (bottom) plotted versus normalized frequency for an 1D periodic medium with inhomogeneities consisting of an Helmholtz resonator in shunt, a section of waveguide, and a flexible plate plate in series in an air background, and $l/L = 0.25$. The *Bloch* parameters correspond to the inhomogeneity being centered in the unit cell, as depicted in the insert of the top panel.

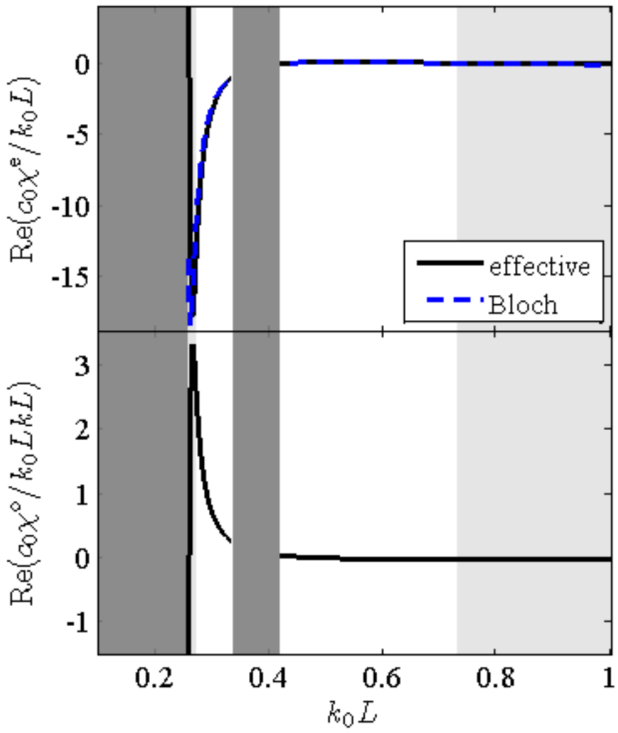

Figure 5.8: Normalized macroscopic even coupling (top) and odd coupling (bottom) plotted versus normalized frequency for an 1D periodic medium with inhomogeneities consisting of an Helmholtz resonator in shunt, a section of waveguide, and a flexible plate plate in series in an air background, and $l/L = 0.25$.

effective even coupling for $k_0L|\mathrm{Re}(kL)| < 0.1$.

5.4 Summary of 1D examples

Three macroscopic descriptions of 1D periodic media were considered: (i) *effective* parameters, which were derived in Chapter 4, relate macroscopic effective fields, and account for Willis coupling due to microscopic asymme-

try and mesoscale effects, (*ii*) *equivalent* parameters that relate macroscopic effective fields but neglect coupling and exist due to non-uniqueness in the absence of sources, and (*iii*) *Bloch* parameters that relate microscopic fields at unit cell boundaries in periodic media. The comparison of *effective* parameters to *equivalent* and *Bloch* parameters was important, because it is often assumed that metamaterials may be described by the same parameters as homogeneous media, leading to *equivalent* parameters, and parameters are often determined by reflection/transmission from a single unit cell or transmission matrices, which results in *Bloch* parameters [22].

For symmetric examples near the quasi-static limit, all three macroscopic descriptions provided similar results, as shown in Figure 5.2, and for asymmetric examples, *Bloch* parameters converged to *effective* parameters when nonlocal effects are negligible, *i.e.*, $(k_0 L)|\mathrm{Re}(kL)| < 0.1$, as shown in Figures 5.4, 5.5, 5.7, and 5.8. Within these limits, reflection/transmission measurements of a single unit cell will lead to meaningful parameters of an infinite periodic medium consisting of the unit cell measured, if the inhomogeneity is centered in the unit cell. Additionally, recent efforts by the author and colleagues beyond this dissertation experimentally verified that even coupling can be measured for an isolated element with negligible odd coupling, and under these experimental constraints, even coupling is given by its leading order expression given in Equation (5.10) [46, 47].

The dynamic features observed for *effective*, *equivalent*, and *Bloch* parameters are consistent with other numerical results in the published literature.

When coupling parameters are included in the homogenization models of Willis [36] and Nemat-Nasser and Srivastava [37], the macroscopic compliance (inverse stiffness, C^{-1}) and density both increase with increasing frequency, *i.e.*, have a positive slopes, but when coupling parameters are absorbed into density and compliance (similar to the *equivalent* parameters) one of these slopes becomes negative indicating a violation of causality. The homogenization model of Yang *et al.* [18] relies on reproducing surface fields and does not account for bianisotropy, and therefore, produces parameters whose imaginary parts may be positive or negative, even though examples are lossless, and real parts with slopes that change sign, indicating causality and passivity violations.

The results of Section 5.3 demonstrate that even though *equivalent* and *Bloch* parameters are useful to describe wave propagation in metamaterials they do not always satisfy fundamental restrictions due to causality and passivity on macroscopic parameters, and therefore, these parameters lack physical meaning. This suggests that the *equivalent* and *Bloch* parameters may not be useful to describe the metamaterial response in the presence of more complex fields, such as in a resonator, and that the use of these parameters could unnecessarily complicate the interpretation of data from experiments or numerical simulations. Therefore, while all three of the models capture wave propagation in inhomogeneous media, the most physically meaningful model would result in macroscopic parameters that strictly obey reciprocity, causality, and passivity on their own, rather than in combination, to describe the overall response of inhomogeneous media.

Chapter 6

Conclusions and Future Directions

6.1 Conclusions and contributions

This dissertation aims to develop an understanding of the microscale and mesoscale origins of bianisotropy in acoustic metametarials, as well as the macroscale observation. Towards these goals, fundamental physical examples are expained and a first-principles homogenization procedure is derived. Chapter 2 provides a brief introduction to bianisotropy in electromagnetism and Willis coupling in elastodynamics in order to highlight physical analogies and promote a qualitative understanding of the origins of bianisotropy in inhomogeneous media. Additionally, qualitative discussions of two effects, microstructure asymmetry and a finite mesoscale, both of which result in bianisotropy being observed in macroscopic wave propagation, are provided. These examples provide an intuitive understanding of the roots of bianisotropy, which is not easily gleened from the present literature.

The microscale and mesoscale origins of bianisotropy are explicitly demostrated by deriving a rigorous source-driven multiple scattering homogenization procedure in Chapter 4. A multiple-scattering scheme is presented because it is more intuitive and lends itself to determining leading order terms,

which significantly aids the analysis in Chapter 5. The resulting *effective* parameters are compared to alternative macroscopic descriptions in light of physical restrictions (derived in Chapter 3) based on assumptions of reciprocal, passive, and causal macroscopic wave propagation in Chapter 5. It is shown that only a model that accounts for coupling due to asymmetry and nonlocal effects satisfies the restrictions on macroscopic parameters. Thus, for macroscopic material properties of acoustic metamaterials to be physically meaningful, one should not neglect bianisotropy; even though the parameters are non-unique in the absence of a source. Additionally, the homogenization procedure and explanation of bianisotropy provided in this dissertation extends the ability to design acoustic metamaterials with unique properties.

The development of this work has contributed to the publication of three conference proceedings, ten conference presentations, and three articles submitted to peer-reviewed journals. The peer-reviewed articles are a recent paper outlining restrictions on properties of local Willis materials [24], a paper accepted for publication concerning the measurement of Willis coupling of a small metamaterial sample [47], and portions of this work were recently submitted as an article demonstrating the origins of Willis coupling in acoustic metamaterials [90].

6.2 Future directions

At this point, bianisotropy in acoustic metamaterials remains primarily an academic curiosity with only one published paper thus far providing an ex-

perimental demonstration and suggesting applications [39]. Therefore, a lot of opportunities remain in the development of acoustic bianisotropy. Two related topics stemming directly from this work are the extension of the homogenization model developed in Chapter 4 to more general lattices and to develop a better understanding of the role of bianisotropy in measurements. This work concludes with a few proposed applications of acoustic bianisotropy.

6.2.1 Model extension

The derivation in Chapter 4 and extensions of it are only valid for small inhomogeneities for which multiple scattering analysis and the polarizability approximation are acceptable. Larger inhomogeneities can be accommodated if one accounts for the acausal response due to their finite size [81]. As presented, the homogenization model may be used to find effective properties of any infinite periodic lattice for which rapidly converging series exist for the interaction coefficients, Equation (4.14). However, to author's knowledge, coupled interaction coefficients have only been expressed for the 1D case presented in Chapter 5, but the results of Shore and Yaghjian [78] suggest that rapidly converging series probably exist for $\boldsymbol{C}_{\mathrm{c}}$ for 2- and 3D cubic lattices. The inhomogeneity response, Equation (4.7), could also be extended to account for nonreciprocal effects and quadrapole moments.

Only being able to determine parameters for infinite cubic lattices is quite restricting, but calculating parameters for finite or arbitrary arrays requires knowledge of local fields at each inhomogeneity. This could possibly be

accomplished by considering an iterative approach to solve Equation (4.12) at each inhomogeneity. If successful, the iterative approach would allow for the homogenization of finite arrays and gradient index metamaterials where the inhomogeneities do not have identical polarizabilities. Polarizabilities of each inhomogeneity would need to be determined *a priori*, and some assumptions would have to be made about the spatial variations of macroscopic parameters. This approach could potentially solve some of the issues related to the ambiguous boundaries of finite lattices [65, 91].

6.2.2 Measurements of acoustic bianisotropy

To date, only acoustic bianisotropy due to asymmetry (even coupling) has been measured for a single unit cell using the reflection/transmission method [39, 47]. Therefore, these experiments measured *Bloch* parameters as discussed in Chapter 5, and the coupling depends on how the boundaries of the measurement sample are defined, as demonstrated in Fig. 5.3. Distinguishing between an intrinsic or irreducible even coupling and that which depends on the boundaries of the sample will likely be a challenging task and require samples composed of multiple unit cells. However, when considering a measurement of multiple unit cells, one will likely need to account for Fabry-Perot artifacts [92], boundary layers [91], and odd coupling.

The measurement of odd coupling has only been demonstrated for very specific conditions in electromagnetism [93], and it has yet to be demonstrated that odd coupling can be measured in general. A better understanding of how

odd coupling impacts propagation and energy flow in acoustic metamaterials would likely inform these procedures, which would involve an energy analysis similar to that of Fietz in electromagnetism that accounts for spatial dispersion as well as temporal dispersion [94].

6.2.3 Applications

Koo *et al.* [39] demonstrated that even coupling can be used for impedance matching and control of transmission and reflection angles from a metasurface, which could be applied to create a diffusive surface. Building upon the analogs to bianisotropy in electromagnetism, one could achieve "acoustic nihility" (counterpart to chiral nihility [54]) in which a zero-index is obtained with finite density and compressiblity. Additionally, a clearer understanding of bianisotropy in acoustics due to microscale and mesoscale effects will inform the design metamaterial based devices, including lenses and cloaks, and could aid non-destructive evaluation and imaging technologies by introducing new ways of accounting for subwavelenth interactions.

Appendices

Appendix A

Green's Functions

The volumetric Dirac delta may be defined for 1-, 2-, and 3D space as

$$\delta_{\boldsymbol{n}} = \begin{cases} \delta(x - x_n)/A & \text{1D}, \\ \delta(x - x_n)\delta(y - y_n)/L_z & \text{2D}, \\ \delta(x - x_n)\delta(y - y_n)\delta(z - z_n) & \text{3D}, \end{cases} \tag{A.1}$$

where A is a representative cross-sectional area and L_z a representative out-of-plane length such that $\delta_{\boldsymbol{n}}$ has units of inverse volume in all three cases presented. The scalar free space Green's function in the reciprocal background medium, $g(\boldsymbol{x}|\boldsymbol{x_n})$, which evaluates the scalar field at the point $\boldsymbol{x}$ due to a unit impulse at $\boldsymbol{x_n}$, is defined by $(\nabla^2 + k_0^2)\, g(\boldsymbol{x}|\boldsymbol{x_n}) = -\delta_{\boldsymbol{n}}$.

The fields due to body force, $\boldsymbol{f}$, and mass source, q, distributions in a volume V are expressed in terms of the scalar Green's function as

$$\begin{aligned} \boldsymbol{u}(\boldsymbol{x}) = -\frac{1}{i\omega\rho_0} \int_{\boldsymbol{y}} \boldsymbol{f}(\boldsymbol{y}) \cdot \nabla\nabla g(\boldsymbol{x}|\boldsymbol{y}) dV \\ - \int_{\boldsymbol{y}} q(\boldsymbol{y}) \nabla g(\boldsymbol{x}|\boldsymbol{y}) dV, \\ p(\boldsymbol{x}) = -i\omega\rho_0 \int_{\boldsymbol{y}} q(\boldsymbol{y}) g(\boldsymbol{x}|\boldsymbol{y}) dV \\ - \int_{\boldsymbol{y}} \boldsymbol{f}(\boldsymbol{y}) \cdot \nabla g(\boldsymbol{x}|\boldsymbol{y}) dV. \end{aligned} \tag{A.2}$$

From these expressions, the scattered fields at a point $\boldsymbol{x_m}$ due to an inhomogeneity located at $\boldsymbol{x_n}$ maybe expressed by Equation (4.10) in terms of the

dipole and monopole moments of the $\boldsymbol{n}$th inhomogeneity by relating the dipole moment to the body force, $\boldsymbol{f} = i\omega \boldsymbol{d_n} \delta_{\boldsymbol{n}}$, and monopole moment to the volume source, $q = -i\omega m_{\boldsymbol{n}} \delta_{\boldsymbol{n}}$. The modifed Green's functions are defined in Equation (4.11).

The scalar Green's functions for 1-, 2-, and 3D are

$$g(\boldsymbol{x}|\boldsymbol{x_n}) = \begin{cases} ie^{ik_0|x-x_n|}/2k_0A & \text{1D}, \\ iH_0^{(1)}(k_0R_2)/4L_z & \text{2D}, \\ e^{ik_0R_3}/4\pi R_3 & \text{3D}, \end{cases} \tag{A.3}$$

where $H_0^{(1)}$ is the zero order Hankel function of the first kind, $R_2 = \sqrt{(x-x_n)^2 + (y-y_n)^2}$, and $R_3 = \sqrt{(x-x_n)^2 + (y-y_n)^2 + (z-z_n)^2}$. Then for 1D, the modified Green's functions reduce to

$$\begin{aligned} \underline{\boldsymbol{G}}_{\mathrm{d}}^{\boldsymbol{mn}} &= \hat{x}\hat{x}\frac{ik_0}{2A}e^{ik_0L|m-n|} = \hat{x}\hat{x}G_{\mathrm{m}}^{\boldsymbol{mn}}, \\ \boldsymbol{G}_{\mathrm{c}}^{\boldsymbol{mn}} &= \pm\hat{x}\frac{ik_0}{2A}e^{ik_0L|m-n|}, \end{aligned} \tag{A.4}$$

where $+\hat{x}$ corresponds to $m > n$ and $-\hat{x}$ to $m < n$.

Appendix B

Scattering Matrix

Consider incident and outgoing acoustic waves at the boundaries of an inhomogeneity. The pressure amplitudes are related via the scattering mattrix as

$$\begin{bmatrix} p_1^{\text{out}} \\ p_2^{\text{out}} \end{bmatrix} = \begin{bmatrix} S_{11} & S_{12} \\ S_{21} & S_{22} \end{bmatrix} \begin{bmatrix} p_1^{\text{in}} \\ p_2^{\text{in}} \end{bmatrix}, \tag{B.1}$$

where the superscripts distinguish incident and outgoing and the subscripts indicate which boundary with p_1 evaluated at $x = -l/2$ and p_2 evaluated at $x = l/2$. A reciprocal inhomogeneity exhibits $S_{12} = S_{21}$, and if the inhomogeneity is also symmetric, then $S_{11} = S_{22}$. Outgoing waves may also be expressed in terms of incident and scattered pressures,

$$\begin{aligned} p_1^{\text{out}} &= p_2^{\text{in}} e^{ik_0 l} + p_{\text{s}}(-l/2) = S_{11} p_1^{\text{in}} + S_{12} p_2^{\text{in}} \\ p_2^{\text{out}} &= p_1^{\text{in}} e^{ik_0 l} + p_{\text{s}}(l/2) = S_{21} p_1^{\text{in}} + S_{22} p_2^{\text{in}}. \end{aligned} \tag{B.2}$$

In the absence of the inhomogeneity, local fields at $x = 0$ are given by the incident fields

$$\begin{aligned} p_{\text{loc}} &= p_1^{\text{in}} e^{ik_0 l/2} + p_2^{\text{in}} e^{ik_0 l/2} \\ \boldsymbol{u}_{\text{loc}} &= \frac{\hat{x}}{Z_0} \left(p_1^{\text{in}} e^{ik_0 l/2} - p_2^{\text{in}} e^{ik_0 l/2} \right). \end{aligned} \tag{B.3}$$

For 1D, evaluating Equation (4.10) at $x = \pm l/2$ leads to

$$\begin{aligned} i\frac{k_0}{A}e^{ik_0 l/2}\ \frac{\boldsymbol{d_0}}{\rho_0} &= \boldsymbol{u}_{\mathrm{s}}(l/2) + \boldsymbol{u}_{\mathrm{s}}(-l/2), \\ -i\frac{k_0}{A}e^{ik_0 l/2}\ \frac{m_{\mathbf{0}}}{\beta_0} &= p_{\mathrm{s}}(l/2) + p_{\mathrm{s}}(-l/2) \end{aligned} \tag{B.4}$$

The polarizablities may be determined using Equation (B.2) and (B.3) in Equation (B.4) to express the monopole and dipole moments in terms of local fields and comparing to Equation (4.7).

Appendix C

Interaction Coefficients

Substituting the 1D modified Green's functions in Equation (A.4) into Equation (4.14), the interaction coefficients become

$$\begin{aligned} C_{\mathrm{m}} &= \frac{ik_0}{2A}\sum_{n=1}^{\infty}\left(e^{-i\boldsymbol{k}\cdot\hat{x}nL}+e^{i\boldsymbol{k}\cdot\hat{x}nL}\right)e^{ik_0nL}, \\ \underline{\boldsymbol{C}}_{\mathrm{d}} &= \hat{x}\hat{x}\frac{ik_0}{2A}\sum_{n=1}^{\infty}\left(e^{-i\boldsymbol{k}\cdot\hat{x}nL}+e^{i\boldsymbol{k}\cdot\hat{x}nL}\right)e^{ik_0nL}, \\ \boldsymbol{C}_{\mathrm{c}} &= \hat{x}\frac{ik_0}{2L}\sum_{n=1}^{\infty}\left(e^{-i\boldsymbol{k}\cdot\hat{x}nL}-e^{i\boldsymbol{k}\cdot\hat{x}nL}\right)e^{ik_0nL}. \end{aligned} \tag{C.1}$$

Equation (5.3) may be obtained using the geometric series rule

$$\sum_{n=1}^{\infty}x^n=\frac{x}{1-x}, \tag{C.2}$$

where $|x|<1$. As discussed by Shore and Yaghjian [78], this approach is valid assuming some small imaginary part of $\boldsymbol{k}$ and k_0, *i.e.*, damping, which is present in all real systems.

Appendix D

Scattered Power Relations

The derivation here is based on the work of Strickland *et al.* [95] for cylindrical scatterers. The restrictions on the complementary polarizabilities will be derived for a single inhomogeneity placed at the origin based on power conservation, *i.e.*, the scattered power cannot exceed the power extracted from the local fields. The power extracted by the inhomogeneity must be positive and is given by

$$\begin{aligned} P_{\mathrm{e}} &= -\frac{1}{2}\mathrm{Re}\left(i\omega \boldsymbol{d_0}\cdot\boldsymbol{u}^*_{\mathrm{loc}} + i\omega m^*_{\mathbf{0}} p_{\mathrm{loc}}\right) \\ &= \frac{\omega}{2}\mathrm{Im}\left(\boldsymbol{d_0}\cdot\boldsymbol{u}^*_{\mathrm{loc}} + m^*_{\mathbf{0}} p_{\mathrm{loc}}\right). \end{aligned} \tag{D.1}$$

For 1D and using Equation (4.12), the extracted power simplifies to

$$P_{\mathrm{e}} = -\frac{\omega}{2}\begin{bmatrix} d_0 & m_0 \end{bmatrix}\cdot\begin{bmatrix} \frac{\mathrm{Im}(\tilde{\alpha}_{\mathrm{d}})}{\rho_0} & \frac{\mathrm{Im}(\tilde{\alpha}_{\mathrm{c}})}{-i/c_0} \\ \frac{\mathrm{Im}(\tilde{\alpha}_{\mathrm{c}})}{i/c_0} & \frac{\mathrm{Im}(\tilde{\alpha}_{\mathrm{m}})}{\beta_0} \end{bmatrix}\cdot\begin{bmatrix} d_0 \\ m_0 \end{bmatrix}^*. \tag{D.2}$$

The total power radiated from the inhomogeneity, determined from the scattered fields, Equation (4.10), may be expressed as

$$\begin{aligned} P_{\mathrm{r}} &= \frac{1}{2}\Re\left(-p_{\mathrm{s}}\boldsymbol{u}^*_{\mathrm{s}}|_{x=-l/2} + p_{\mathrm{s}}\boldsymbol{u}^*_{\mathrm{s}}|_{x=l/2}\right)\cdot\hat{x}A \\ &= \frac{\omega}{2}\frac{k_0}{2A}\begin{bmatrix} d_0 & m_0 \end{bmatrix}\cdot\begin{bmatrix} 1/\rho_0 & 0 \\ 0 & 1/\beta_0 \end{bmatrix}\cdot\begin{bmatrix} d_0 \\ m_0 \end{bmatrix}^*. \end{aligned} \tag{D.3}$$

For a passive inhomogeneity, $P_{\mathrm{e}} \geq P_{\mathrm{r}}$, which leads to $\mathrm{Im}(\tilde{\alpha}_{\mathrm{d}}) \leq -k_0/2A$ and $\mathrm{Im}(\tilde{\alpha}_{\mathrm{m}}) \leq -k_0/2A$, where equality only occurs for a lossless inhomogeneity,

and $\mathrm{Im}(\tilde{\alpha}_{\mathrm{c}}) = 0$ for a lossless inhomogeneity. Additionally, since $P_{\mathrm{e}} - P_{\mathrm{r}} \geq 0$, the matrix

$$\begin{bmatrix} -\left(\frac{k_0}{2A} + \mathrm{Im}(\tilde{\alpha}_{\mathrm{d}})\right)/\rho_0 & -ic_0\mathrm{Im}(\tilde{\alpha}_{\mathrm{c}}) \\ ic_0\mathrm{Im}(\tilde{\alpha}_{\mathrm{c}}) & -\left(\frac{k_0}{2A} + \mathrm{Im}(\tilde{\alpha}_{\mathrm{m}})\right)/\beta_0 \end{bmatrix}$$

must be positive definite, requiring

$$\mathrm{Im}(\tilde{\alpha}_{\mathrm{c}})^2 \leq \left(\frac{k_0}{2A} + \mathrm{Im}(\tilde{\alpha}_{\mathrm{d}})\right)\left(\frac{k_0}{2A} + \mathrm{Im}(\tilde{\alpha}_{\mathrm{m}})\right). \tag{D.4}$$

Bibliography

[1] J. B. Pendry. Negative refraction makes a perfect lens. *Phys. Rev. Lett.*, 85(18):3966–3969, 2000.

[2] D. R. Smith, Willie J. Padilla, D. C. Vier, S. C. Nemat-Nasser, and S. Schultz. Composite medium with simultaneously negative permeability and permittivity. *Phys. Rev. Lett.*, 84(18):4184–4187, 2000.

[3] Z. Liu, X. Zhang, Y. Mao, Y. Y. Zhu, Z. Yang, C. T. Chan, and P. Sheng. Locally resonant sonic materials. *Science*, 289(5485):1734–1736, 2000.

[4] V. M. Byrdin. On the centenary of the pioneering study on backward waves: the beginnings and development of backward-wave mechanics and electromagnetics. *J. Commun. Technol. Electron.*, 50(12):1307, 2005.

[5] C. R. Simovski and S. A. Tretyakov. Historical notes on metamaterials. In F. Capolino, editor, *Theory and Phenomena of Metamaterials*, Metamaterials Handbook, chapter 1. Taylor & Francis, 2009.

[6] M. Kadic, T. Bückmann, R. Schittny, and M. Wegener. Metamaterials beyond electromagnetism. *Rep. Prog. Phys.*, 76(12):126501, 2013.

[7] R. Fleury and A. Alù. Cloaking and invisibility: a review. *FERMAT*, 1 (7):1–24, 2014.

[8] X. Zhang and Z. Liu. Superlenses to overcome the diffraction limit. *Nat. Mater.*, 7(6):435–441, 2008.

[9] M. R. Haberman and M. D. Guild. Acoustic metamaterials. *Physics Today*, 69(6):42–48, 2016.

[10] S. A. Cummer, J. Christensen, and A. Alù. Controlling sound with acoustic metamaterials. *Nat. Rev. Mater.*, 1:16001, 2016.

[11] G. Ma and P. Sheng. Acoustic metamaterials: From local resonances to broad horizons. *Sci. Adv.*, 2(2):e1501595, 2016.

[12] M. Dubois, C. Shi, X. Zhu, Y. Wang, and X. Zhang. Observation of acoustic dirac-like cone and double zero refractive index. *Nat. Commun.*, 8:14871, 2017.

[13] D. R. Smith and J. B. Pendry. Homogenization of metamaterials by field averaging. *J. Opt. Soc. Am. B*, 23(3):391–403, 2006.

[14] C. Fietz and G. Shvets. Current-driven metamaterial homogenization. *Physica B*, 405(14):2930–2934, 2010.

[15] A. Alù. First-principles homogenization theory for periodic metamaterials. *Phys. Rev. B*, 84(7):075153, 2011.

[16] J. R. Willis. Effective constitutive relations for waves in composites and metamaterials. *Proc. R. Soc. A*, 467(2131):1865–1879, 2011.

[17] A. N. Norris, A. L. Shuvalov, and A. A. Kutsenko. Analytical formulation of three-dimensional dynamic homogenization for periodic elastic systems. *Proc. R. Soc. A*, 468(2142):1629–1651, 2012.

[18] M. Yang, G. Ma, Y. Wu, Z. Yang, and P. Sheng. Homogenization scheme for acoustic metamaterials. *Phys. Rev. B*, 89(6):064309, 2014.

[19] D. Torrent, Y. Pennec, and B. Djafari-Rouhani. Resonant and nonlocal properties of phononic metasolids. *Phys. Rev. B*, 92(17):174110, 2015.

[20] M. A. Gorlach, T. A. Voytova, M. Lapine, Y. S. Kivshar, and P. A. Belov. Nonlocal homogenization for nonlinear metamaterials. *Phys. Rev. B*, 93 (16):165125, 2016.

[21] M. B. Muhlestein and M. R. Haberman. A micromechanical approach for homogenization of elastic metamaterials with dynamic microstructure. *Proc. R. Soc. A*, 472(2192):20160438, 2016.

[22] C. R. Simovski. On electromagnetic characterization and homogenization of nanostructured metamaterials. *J. Opt.*, 13(1):013001, 2011.

[23] A. Alù. Restoring the physical meaning of metamaterial constitutive parameters. *Phys. Rev. B*, 83(8):081102, 2011.

[24] M. B. Muhlestein, C. F. Sieck, A. Alù, and M. R. Haberman. Reciprocity, passivity, and causality in Willis materials. *Proc. R. Soc. A*, 472(2194): 20160604, 2016.

[25] J.-A. Kong. Theorems of bianisotropic media. *Proc. IEEE*, 60(9):1036–1046, 1972.

[26] I. V. Lindell, A. H. Sihvola, S. A. Tretyakov, and A. J. Viitanen. *Electromagnetic Waves in Chiral and Bi-isotropic Media*. Artech House, 1994.

[27] J. R. Willis. Polarization approach to the scattering of elastic waves—I. Scattering by a single inclusion. *J. Mech. Phys. Solids*, 28(5):287–305, 1980.

[28] J. R. Willis. Variational principles for dynamic problems for inhomogeneous elastic media. *Wave Motion*, 3(1):1–11, 1981.

[29] J. R. Willis. The nonlocal influence of density variations in a composite. *Int. J. Solids Struct.*, 21(7):805–817, 1985.

[30] G. W. Milton and J. R. Willis. On modifications of newton's second law and linear continuum elastodynamics. *Proc. R. Soc. A*, 463(2079): 855–880, 2007.

[31] A. Srivastava. Elastic metamaterials and dynamic homogenization: a review. *Int. J. Smart Nano Mater.*, 6(1):41–60, 2015.

[32] A. Lakhtakia, V. K. Varadan, and V. V. Varadan. *Time-Harmonic Electromagnetic Fields in Chiral Media*. Springer-Verlag, 1989.

[33] V. V. Varadan, A. Lakhtakia, and V. K. Varadan. Geometry can be the basis for acoustic activity (*a la* optical activity) in composite media. *J. Wave-Mater. Interact.*, 1(3):315–324, 1986.

[34] M. M. I. Saadoun and N. Engheta. A reciprocal phase shifter using novel pseudochiral or Ω medium. *Microw. Opt. Technol. Lett.*, 5(4):184–188, 1992.

[35] D. A. Powell and Y. S. Kivshar. Substrate-induced bianisotropy in metamaterials. *Appl. Phys. Lett.*, 97:091106, 2010.

[36] J. R. Willis. Exact effective constitutive relations for dynamics of a laminated body. *Mech. Mater.*, 41:385–393, 2009.

[37] S. Nemat-Nasser and A. Srivastava. Overall dynamic constitutive relations of layered elastic composites. *J. Mech. Phys. Solids*, 59(10):1953–1965, 2011.

[38] H. Nassar, Q.-C. He, and N. Auffray. Willis elastodynamic homogenization theory revisited for periodic media. *J. Mech. Phys. Solids*, 77:158–178, 2015.

[39] S. Koo, C. Cho, J.-h. Jeong, and N. Park. Acoustic omni meta-atom for decoupled access to all octants of a wave parameter space. *Nat. Commun.*, 7:13012, 2016.

[40] C. F. Sieck, A. Alù, and M. R. Haberman. Dynamic homogenization of acoustic metamaterials with coupled field response. *Phys. Procedia*, 70: 275–278, 2015.

[41] M.-F. Ponge, O. Poncelet, and D. Torrent. Dynamic homogenization theory for nonlocal acoustic metamaterials. *Extreme Mech. Lett.*, 12:71–76, 2017.

[42] B. D. H. Tellegen. The gyrator, a new electric network element. *Philips Res. Rep.*, 3(2):81–101, 1948.

[43] L.-Q. Shui, Z.-F. Yue, Y.-S. Liu, Q.-C. Liu, J.-J. Guo, and X.-D. He. Novel composites with asymmetrical elastic wave properties. *Compos. Sci. Technol.*, 113:19–30, 2015.

[44] H. Nassar, X.C. Xu, A. N. Norris, and G. L. Huang. Modulated phononic crystals: Non-reciprocal wave propagation and Willis materials. *J. Mech. Phys. Solids*, 101:10–29, 2017.

[45] C. R. Simovski. On the extraction of local material parameters of metamaterials from experimental or simulated data. In F. Capolino, editor, *Theory and Phenomena of Metamaterials*, Metamaterials Handbook, chapter 11. Taylor & Francis, 2009.

[46] M. B. Muhlestein. *Willis Coupling in Acoustic and Elastic Metamaterials*. PhD thesis, The University of Texas at Austin, 2016.

[47] M. B. Muhlestein, C. F. Sieck, P. S. Wilson, and M. R. Haberman. Experimental evidence of Willis coupling in one-dimensional effective material element. *Nat. Commun.*, (accepted), 2017.

[48] D. K. Cheng and J.-A. Kong. Covariant descriptions of bianisotropic media. *Proc. IEEE*, 56(3):248–251, 1968.

[49] K. F. Lindman. Om en genom ett isotropt system av spiralformiga resonatorer alstrad rotationspolarisation av de elektromagnetiska vågorna. *Öfversigt af Finska Vetenskaps-Societetens förhandlingar, A*, LVII(3):1–32, 1914.

[50] L. D. Landau and E. M. Lifshitz. *Electrodynamics of continuous media*. Pergamon Press, 1960.

[51] S. A. Tretyakov. A personal view on the origins and developments of the metamaterials concept. *J. Opt.*, 19(1):013002, 2017.

[52] M. M. I. Saadoun and N. Engheta. Theoretical study of electromagnetic properties of non-local Ω media. *PIER*, 9:351–397, 1994.

[53] D. Ramaccia, L. Di Palma, D. Ates, E. Ozbay, A. Toscano, and F. Bilotti. Analytical model of connected bi-omega: Robust particle for the selective power transmission through sub-wavelength apertures. *IEEE Trans. Antennas and Propag.*, 62(4):2093–2101, 2014.

[54] C.-W. Qiu, Z. Saïd, and A. Sihvola. A review of chiral and bianisotropic composite materials providing backward waves and negative refractive indices. In F. Capolino, editor, *Theory and Phenomena of Metamaterials*, Metamaterials Handbook, chapter 24. Taylor & Francis, 2009.

[55] A. A. Andronov. On the natural rotation of polarization plane of sound. *Izv. Vyssh. Uchebn. Zaved., Radiofiz*, 3:645, 1960.

[56] V. P. Silin. Contribution to the theory of absorption of ultrasound in metals. *Sov. Phys. JETP*, 11(3):703, 1960.

[57] G. Kluge and G. Scholz. Die drehung der polarisationsebene von transversalen schallwellen. *Acta Acust. united Ac.*, 16(1):60–64, 1965.

[58] D. L. Portigal and E. Burstein. Acoustical activity and other first-order spatial dispersion effects in crystals. *Phys. Rev.*, 170(3):673–678, 1968.

[59] A. S. Pine. Direct observation of acoustical activity in α quartz. *Phys. Rev. B*, 2(6):2049–2054, 1970.

[60] K. F. Tee, A. Spadoni, and M. Scarpa, F. Ruzzene. Wave propagation in auxetic tetrachiral honeycombs. *ASME J. Vib. Acoust.*, 132(3):031007, 2010.

[61] R. Wunenburger, J. I. V. Lozano, and E. Brasselet. Acoustic orbital angular momentum transfer to matter by chiral scattering. *New J. Phys.*, 17(10):103022, 2015.

[62] J. Dubois, C. Aristégui, and O. Poncelet. Spaces of electromagnetic and mechanical constitutive parameters for dissipative media with either positive or negative index. *J. Appl. Phys.*, 115(2):024902, 2014.

[63] B. Banerjee. *An Introduction to Metamaterials and Waves in Composites*. CRC Press, 2011.

[64] A. Srivastava. Causality and passivity in elastodynamics. *Proc. R. Soc. A*, 471(2180):20150256, 2015.

[65] V. Fokin, M. Ambati, C. Sun, and X. Zhang. Method for retrieving effective properties of locally resonant acoustic metamaterials. *Phys. Rev. B*, 76(14):144302, 2007.

[66] Z. G. Wang, S. H. Lee, C. K. Kim, C. M. Park, K. Nahm, and S. A. Nikitov. Effective medium theory of the one-dimensional resonance phononic crystal. *J. Phys. Condens. Matter*, 20(5):055209, 2008.

[67] D. T. Blackstock. *Fundamentals of Physical Acoustics*. John Wiley & Sons, 2000.

[68] F. V. Hunt. Notes on the exact equations governing the propagation of sound in fluids. *J. Acoust. Soc. Am.*, 27(6):1019–1039, 1955.

[69] F. Guerin. Energy dissipation and absorption in reciprocal bi-isotropic media described by different formalisms. *PIER*, 9:31–44, 1994.

[70] A. D. Pierce. *Acoustics: An Introduction to Its Physical Principles and Applications*. Acoustical Society of America, 1989.

[71] P. M. Morse and K. U. Ingard. *Theoretical Acoustics*. McGraw-Hill, 1968.

[72] I.V. Lindell. *Methods for Electromagnetic Field Analysis*. Oxford University Press, 1992.

[73] A. Welters, Y. Avniel, and S. G. Johnson. Speed-of-light limitations in passive linear media. *Phys. Rev. A*, 90:023847, 2014.

[74] M. O'Donnell, E. T. Jaynes, and J. G. Miller. Kramers-Kronig relationship between ultrasonic attenuation and phase velocity. *J. Acoust. Soc. Am.*, 69(3):696–701, 1981.

[75] V. Twersky. Acoustic bulk parameters of random volume distributions of small scatterers. *J. Acoust. Soc. Am.*, 36(7):1314–1329, 1964.

[76] V. Twersky. Acoustic bulk parameters in distributions of pair-correlated scatterers. *J. Acoust. Soc. Am.*, 64(6):1710–1719, 1978.

[77] D. Torrent and J. Sánchez-Dehesa. Multiple scattering formulation of two-dimensional acoustic and electromagnetic metamaterials. *New J. Phys.*, 13(9):093018, 2011.

[78] R. A. Shore and A. D. Yaghjian. Traveling waves on two- and three-dimensional periodic arrays of lossless scatterers. *Radio Sci.*, 42(6): RS6S21, 2007.

[79] D. M. Pozar. *Microwave Engineering*. John Wiley & Sons, third edition, 2004.

[80] C. E. Bradley. Time harmonic acoustic bloch wave propagation in periodic waveguides. Part II. Experiment. *J. Acoust. Soc. Am.*, 96(3):1854–1862, 1994.

[81] A. Alù, A. D. Yaghjian, R. A. Shore, and M. G. Silveirinha. Causality relations in the homogenization of metamaterials. *Phys. Rev. B*, 84(5): 054305, 2011.

[82] L. Brillouin. *Wave Propagation in Periodic Structures: Electric Filters and Crystal Lattices*. Dover, 2003.

[83] A. A. Kutsenko, A. L. Shuvalov, O. Poncelet, and A. N. Darinskii. Tunable effective constants of the one-dimensional piezoelectric phononic crystal with internal connected electrodes. *J. Acoust. Soc. Am.*, 137(2):606–616, 2015.

[84] F. Bongard, H. Lissek, and J. R. Mosig. Acoustic transmission line metamaterial with negative/zero/positive refractive index. *Phys. Rev. B*, 82 (9):094306, 2010.

[85] Y. M. Seo, J. J. Park, S. H. Lee, C. M. Park, C. K. Kim, and S. H. Lee. Acoustic metamaterial exhibiting four different sign combinations of density and modulus. *J. Appl. Phys.*, 111(2):023504, 2012.

[86] N. Kim, Y.-J. Yoon, and J. B. Allen. Generalized metamaterials: Definitions and taxonomy. *J. Acoust. Soc. Am.*, 139(6):3412–3418, 2016.

[87] C. E. Bradley. Time harmonic acoustic bloch wave propagation in periodic waveguides. Part I. Theory. *J. Acoust. Soc. Am.*, 96(3):1844–1853, 1994.

[88] A. Srivastava and S. Nemat-Nasser. On the limit and applicability of dynamic homogenization. *Wave Motion*, 51(7):1045–1054, 2014.

[89] N. Fang, D. Xi, J. Xu, M. Ambati, W. Srituravanich, C. Sun, and X. Zhang. Ultrasonic metamaterials with negative modulus. *Nat. Mater.*, 5(6):452–456, 2006.

[90] C. F. Sieck, A. Alù, and M. R. Haberman. Origins of Willis coupling (bianisotropy) in acoustic metamaterials through source-driven homogenization. (in review), 2017.

[91] J. H. Park, H. J. Lee, and Y. Y. Kim. Characterization of anisotropic acoustic metamaterial slabs. *J. Appl. Phys.*, 119(3):034901, 2016.

[92] X.-X. Liu, D. A. Powell, and A. Alù. Correcting the Fabry-Perot artifacts in metamaterial retrieval procedures. *Phys. Rev. B*, 84(23):235106, 2011.

[93] X.-X. Liu and A. Alù. Generalized retrieval method for metamaterial constitutive parameters based on a physically driven homogenization approach. *Phys. Rev. B*, 87(23):235136, 2013.

[94] C. R. Fietz. *Homogenization of Metamaterials with Spatial Dispersion.* PhD thesis, The University of Texas at Austin, 2011.

[95] D. Strickland, A. Ayón, and A. Alù. Dynamic polarizability tensor for circular cylinders. *Phys. Rev. B*, 91(8):085104, 2015.